Journal of Energy Storage 84 (2024) 110818

Contents lists available at ScienceDirect

Journal of Energy Storage

journal homepage: www.elsevier.com/locate/est

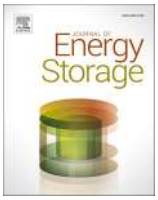

Research papers

# Thermodynamic analysis of heat storage of ocean thermal energy conversion integrated with a two-stage turbine by thermal power plant condenser output water

Siamak Hoseinzadeh [a,*,1], Mehdi Asadi PaeinLamouki [b,1], Davide Astiaso Garcia [a]

[a] Department of Planning, Design, and Technology of Architecture, Sapienza University of Rome, Via Flaminia 72, 00196 Rome, Italy
[b] Faculty of Engineering, Amol University of Special Modern Technologies, Amol, Iran

ARTICLE INFO

*Keywords:*
Heat storage
Energy and exergy analysis
Thermal efficiency
Ocean thermal energy conversion (OTEC)
Combined Cycle Power Plant (CCPP)
Freshwater

ABSTRACT

The ocean thermal energy conversion (OTEC) system uses the temperature difference between warm sea surface water and deep cold water to generate electrical power. Due to the low-temperature difference between surface warm water and deep-sea cold water, the thermal efficiency of these systems is low compared to fossil fuel-driven power plants. In the present study, to propose a method for increasing the output power, thermal efficiency, and heat storage of an OTEC cycle, the warm water outlet of the existing thermal power plant is used instead of surface water which is conventionally employed in basic OTEC cycles. The results show that, considering average electrical net power in the basic OTEC cycle per month the energy and exergy efficiencies are 3.34 % and 17.2 %, respectively. Then, the suggested OTEC cycle is investigated using a two-stage turbine and reheating in terms of energy and exergy. Comparing the results obtained for the two configurations shows that, in the proposed cycle, the average output power is increased by 552 kWh per month, and energy and exergy efficiencies are improved by 0.048 % and 0.31 %, respectively. As an existing thermal cycle performance, a case study of a real Combined Cycle Power Plant (CCPP) is modeled with the proposed cycle. The results show that the average net electrical power is produced by 17.72 MWh per month by using the outlet water from the condenser of CCPP and the energy and exergy efficiencies have been increased by 1.432 % and 8.02 %, respectively Compared to the base cycle. Also, using condenser outlet warm water, an average of 18,829 tons per day of fresh water is produced, and the thermal efficiency of the CCPP is improved by 1.87 %.

## 1. Introduction

Energy supply has been one of the essential prerequisites for economic development and improvement of human life's quality throughout history. The growing population of the planet and the growing need of human beings for energy in the early 21st century have led to an increase in the importance of energy supply and posed an energy crisis. The situation has led to significant efforts by developed industrial countries to find effective and more environmentally friendly solutions in order to respond to the growing energy need and manage the energy crisis. Despite the made efforts, traditional energy sources, i.e., fossil fuels, nuclear fission, and large hydropower, and their harmful effects such as global warming and environmental pollution [1] have become more apparent in recent years and dominated the global energy supply chain. In addition, other sources of electricity production from renewable energy sources like the extraction of latent energy in the seas and oceans have drawn much attention. As a result, and aligned with European nations, like Italy, that have actively relied on renewable energy as the main source of electricity generation, the significant role of renewable energy in the global energy supply chain in the coming years is undeniable and unavoidable [2–4].

Among a variety of renewable energy sources including solar, wind, geothermal, organic material, biofuels, and various forms of marine energy, the seas and oceans are one of the most important and powerful sources of renewable energy, mainly because oceans and seas cover about 71 % of the total land surface, receiving significant sun radiant energy, storing significant energy in the form of wave, tides, currents, salinity gradients, and thermal gradient that Soto and Vergara show it in their research significantly [5]. As a result, the developed countries of

* Corresponding author.
*E-mail address:* siamak.hosseinzadeh@uniroma1.it (S. Hoseinzadeh).
[1] These authors contributed equally to this article as the first authors.

https://doi.org/10.1016/j.est.2024.110818
Received 28 October 2023; Received in revised form 25 December 2023; Accepted 1 February 2024

**Nomenclature**

| | |
|---|---|
| $\dot{E}_X$ | Exergy rate (kW) |
| ex | Specific exergy (kW/kg) |
| H | Enthalpy (kJ) |
| h | Specific enthalpy (kJ/kg) |
| $\dot{I}$ | Exergy destruction rate (kW) |
| $\dot{m}$ | Mass flow rate (kg/s) |
| $\dot{Q}$ | Heat transfer rate (kW) |
| q | Specific heat transfer rate (kW/kg) |
| R | Universal gas constant (J/mol-K) |
| s | Specific entropy (kJ/kg-K) |
| T | Temperature (°C) |
| $\dot{W}$ | Power (kW) |

*Subscripts*

| | |
|---|---|
| 0 | Dead state condition |
| C | Condenser |
| ch | Chemical |
| CP | Cold seawater pump |
| cth | Close-type heater |
| DC | Desalination condenser |
| EDP | Exergy destruction percentage |
| FE | Flash evaporator |
| G | Generator |
| HPE | High pressure evaporator |
| HPT | High pressure turbine |
| in | Inlet |
| loss | Loss |
| LPE | Low pressure evaporator |
| LPT | Low pressure turbine |
| MCH | Mixing chamber |
| net | Net |
| out | Outlet |
| oth | Open-type heater |
| ph | Physical |
| WFP | Working fluid pump |
| WP | Hot seawater pump |
| Q | Heat transfer |
| W | Work |

*Greek*

| | |
|---|---|
| $\eta$ | Efficiency (%) |
| $\Delta$ | Difference |

the world have established comprehensive programs to extract energy by utilizing Ocean thermal energy conversion (OTEC) methods from seas and oceans [6]. In the aquatic environment, solar energy absorbs, stores, and warms the surface water of oceans, however, deep waters of oceans have much lower temperatures. Marine or ocean thermal energy is originated from the temperature difference between warm surface water and cold deep water. In an OTEC power plant, the temperature difference between warm surface water and cold seawater is used in a Rankine cycle to generate power. In other words, the system is a technology that indirectly converts solar irradiation into electricity [7,8]. Therefore, tropical climates provide ideal conditions for OTEC power plants and such locations with this capability can be useful for these systems [9]. Although this energy resource is very vast, however, due to the relatively small temperature difference between the heating and cooling source [10] the thermal efficiency in such cycles with a temperature difference of 20 °C would be about 3 % to 5 %, which is considered low compared to that of thermal power plants using fossil fuels [11,12].

In order to overcome this drawback and enhance the efficiency of the OTEC system, main approaches including, finding proper working fluid [13–19], altering the temperature of the sources, combining the OTEC with other systems, and parameter optimization can be performed. However, in this research, we have not considered the first two of the mentioned enhancing approaches and we are satisfied with a brief explanation. Based on the mechanisms of this system it is obvious that choosing suitable working fluids with decent thermodynamic properties like ammonia, which is repeatedly reported as one of the most suitable working fluids, could significantly improve the efficiency of the system [16]. In addition, increasing the temperature of sources [20], reclaiming energy losses [21], increasing the temperature difference by raising the temperature of the heat source beyond the operating temperature of the cycle and using the output warm water from the condenser of the thermal power plant instead of sea level water lead to improving the performance of the OTEC cycle, enhancing thermal efficiency of the main power plant and elimination of the environmental problems caused by the discharge of high-volume warm water into sea [22].

Integration of OTEC systems with other power sources or other technologies like solar power, fossil fuel systems, wind turbines, and membranes are methods that lead to improving the efficiency and performance of the system [23]. Soto and Vergara investigated the increase in thermal power plant efficiency using an OTEC power plant combined with a 740 MW coal-fired power plant. By using the condenser outlet water, the output power increased by about 25 to 37 MW depending on the seasons. The system was also able to produce 5.8 million tons of fresh water per year. The thermal efficiency of the proposed OTEC system reached 3.4 % and the net efficiency of its main thermal power plant increased by 1.3 % [5]. Yuan et al. investigated an OTEC system based on solar energy. The results of the overall analysis showed that the factors influencing the performance of the pressure generator system are the solar collector output temperature [24]. Ahmadi et al. proposed an OTEC plant combined with solar energy to produce hydrogen. Their system's components included a condenser, turbine, pump, solar collector, and polymer exchange membrane (PEM) and the thermal efficiency and exergy efficiency of the system was about 3.6 % and 22.7 %, respectively [25]. Khosravi et al. proposed a renewable and sustainable energy supply system for remote islands and areas, comprising an OTEC system, a photovoltaic system, and a hydrogen storage system. Energy, exergy, and economic analyses for different working fluids were used to evaluate the proposed hybrid system. The results showed that the maximum output power of the OTEC cycle was obtained for ammonia while the total thermal efficiency of the combined system was 3.318 % [26].

Khanmohammadi et al. analyzed the energy and exergy of an OTEC system. The results showed that adding solar panels to the system increases the exergy efficiency by 6.27 % [27]. Temiz and Dincer analyzed the energy and exergy of a combined OTEC system having a Rankine ammonia cycle, solar panels, a membrane desalination system, and a fuel cell to produce fuel, energy, water, and food in polar regions. The results showed that the overall efficiency of energy and exergy efficiencies were 16.28 % and 36.35 %, respectively [28]. Yilmaz analyzed the energy and exergy of an OTEC system and its combination with a wind turbine power plant in Turkey. It was shown that the energy and exergy efficiency of the OTEC system were 4.49 and 14.84 %, respectively [29]. Ahmadi et al. performed energy, exergy, and economic analyses of different proposed systems for cooling, electricity, hydrogen, and freshwater production based on an OTEC cycle. The results exhibited that increasing the flow rate of warm surface water reduced the exergy efficiency of the system by about 15 % due to an increase in the exergy input of the system, while, at the same time, it increased the net power production of the system [30]. Wang et al. investigated the

utilization of an OTEC in a low-pressure flash evaporation desalination system. In that research, they investigated several performance indicators, including specific electrical energy consumption (SEEC) and recovery ratio (RR). The results indicated that SEEC increased with increasing seawater flow rate. Also, in the conditions where the warm sea water was 30 °C and the deep cold seawater was 8 °C, the system had the maximum water efficiency, and in those conditions, SEEC and RR were 0.126 kWh/kg and 1.5 %, respectively [31].

As mentioned before, another way to improve an OTEC cycle's efficiency is thermodynamic cycle analysis and optimizing its parameters. Malik et al. used multi-objective optimization of the thermodynamic model for enhancing the combination of OTEC and renewable energy and figured out that utilizing thermoelectric in such a system could improve output power, exergy rate, and system stability [32]. Hoseinzadeh et al. used EES software and response level multi-objectives optimization to find the best set of objectives for Bushehr city in Iran and the optimized system while the production of 429,000 m3/h of fresh water was capable of increasing the exergy efficiency to 13.25 % [33]. Gao et al. utilized a two-layer optimization model and improved the efficiency of cooling, heating, and power systems for rural scenarios [34]. Jung et al. analyzed an OTEC system using a thermos-economic perspective and showed that the cost of generating electricity for an OTEC power plant with an output power of 20 kW, was $ 0.363 per kilowatt-hour [35]. Liu et al. examined the optimization of turbines of an OTEC system by a non-parametric model based on the Gaussian process. It was shown that, based on this model, the system was more efficient and had higher efficiency [36]. Optimization based on economic performance has also been performed in a few studies, for instance, Wang et al. addressed the multi-objective optimization of levelized cost of energy (LCOE) and exergy efficiency of an OTEC system. In that research, different working fluids, such as R717, R152a, R134a, R227ea, R600a, and R601, were used. The research results showed that R717 and R601 had the best performance. The results associated with R717 for LCOE and exergy efficiency were 0.34 $/kWh and 28.17 %, respectively, and the corresponding results of R601 were 0.52$/kWh and 28.47 % [37].Yi et al. investigated an OTEC system operated by a pre-expansion ejector absorption power cycle. The results of thermodynamic analysis by MATLAB software showed that the output work of the turbine increased by 79.38 % with the addition of the ejector before expansion [38]. Fan and Chen comprehensively optimized the thermodynamic and economic performance of the OTEC and provided a thermos dynamic model [39].

Because of the high capabilities of the OTEC system, in addition to the mentioned categorized methods in terms of improving the performance of this system, other research has also been conducted in terms of finding more favorable locations, pump shutdown conditions, or unusual applications. Wang et al. investigated the possibility of using OTEC systems to supply energy to underwater vehicles. They used phase change materials to obtain the thermal energy of the ocean surface. The results of their energy modeling and analysis showed that the maximum and average efficiency of energy conversion was 0.55 % and 0.396 %, respectively. Through these results, it was determined that these systems were suitable for supplying energy to vehicles under the ocean [40]. Assareh et al. analyzed the location measurement of an OTEC system in the southwest of Iran. The results of their research exhibited that the system performed best in summer weather conditions and could have an output power of 1,192,607.9 kW per year [41]. Lim et al. simulated the possible conditions and proposed utilizing two refrigerant pumps and two surface seawater and deep water pumps to prevent system shutdown [42].

Considering the fact that the OTEC systems are not well developed and many objectives must be investigated in order to introduce this system into the commercial application vastly and considering the present short comes and its high initial cost required, this system is superior to wind and solar energy stability [43]. This means by delving into the enhancement systems and/or their integration with other sources; access to a more environmentally friendly and reliable electricity generation system is applicable.

In the present study, warm water output from a thermal power plant condenser will be used instead of surface water. This can be regarded as a method to increase efficiency and improve OTEC cycle performance. Also, considering that the two-stage expansion process and the use of reheating will increase the generated capacity, therefore, in this study, single-stage turbines in a normal OTEC cycle is replaced with a two-stage turbine with reheating between stages. The performance of a new and proposed OTEC cycle will be evaluated to figure out the performance improvement of an OTEC technology. In the next step, the model of the system is developed for energy and exergy analyses. Next, the comparison of the extraction modeling results and the results of the proposed cycle with the basic cycle is done. Moreover, as a case study, the use of the OTEC power plant in Iran is investigated using warm water output from the condenser of the combined cycle power plant (CCPP). Through the case study, the possibility of using the proposed OTEC cycle with the Caspian Sea water and warm water output from the condenser of the CCPP having a volume flow of >39 thousand cubic meters per hour and a temperature difference of 10 °C between the reciprocating water of the condenser will be examined. Finally, the effect of using the proposed OTEC cycle on increasing the exergy efficiency of the CCPP is analyzed.

## 2. OTEC cycle

### 2.1. Basic proposed OTEC cycle

Fig. 1 shows a schematic of the OTEC Combined Cycle using the warm water condenser output of a thermal power plant instead of surface warm water. This system, which we call the basic OTEC cycle, is proposed by Soto and Vergara [5] in combination with a 740 MW coal power plant in Chile. This cycle consists of two parts: power generation and freshwater production. The power generation section consists of a closed Rankine cycle operated by ammonia as a working fluid. In this part, at the first step, the ammonia in the evaporator exchanges heat with the warm water of the condenser outlet, coming from the thermal power plant, and then enters the turbine in the state of saturated vapor. This vapor expands in the turbine where power is generated and enters the condenser where the ammonia vapor condenses after transferring heat to cold water from the deep part of the sea. The liquid ammonia coming from the condenser is then sent back to the evaporator via the pump where it closes the cycle.

In the freshwater production section, the warm seawater enters a flash evaporator after leaving the evaporator, the internal pressure of which is kept lower than the ambient pressure by a vacuum pump. The seawater then evaporates due to pressure reduction of the inlet water to the flash evaporator. The produced vapor enters the desalination condenser and condenses by transferring heat to cold seawater. Finally, part of the warm seawater that has not been evaporated in the flash evaporator is discharged to the sea at the flash evaporator temperature. Through this method, the thermal waste caused by the discharge of warm water at high temperature will be greatly reduced.

### 2.2. New proposed OTEC cycle

As mentioned above, due to the low-temperature difference between cooling and heating sources in the OTEC cycle, the thermal efficiency of this power plant is low compared to fossil fuel driven power plants. One approach to increase thermal efficiency is to raise the temperature of the heating source by employing the waste heat of the condenser of the thermal power plant. In this section, the OTEC combined cycle with a two-stage turbine and reheating will be modeled thermodynamically using the EES software, which is especially designed for solving thermodynamic problems. For this purpose, mass, energy, and exergy balance relationships of different components of the cycle are written and

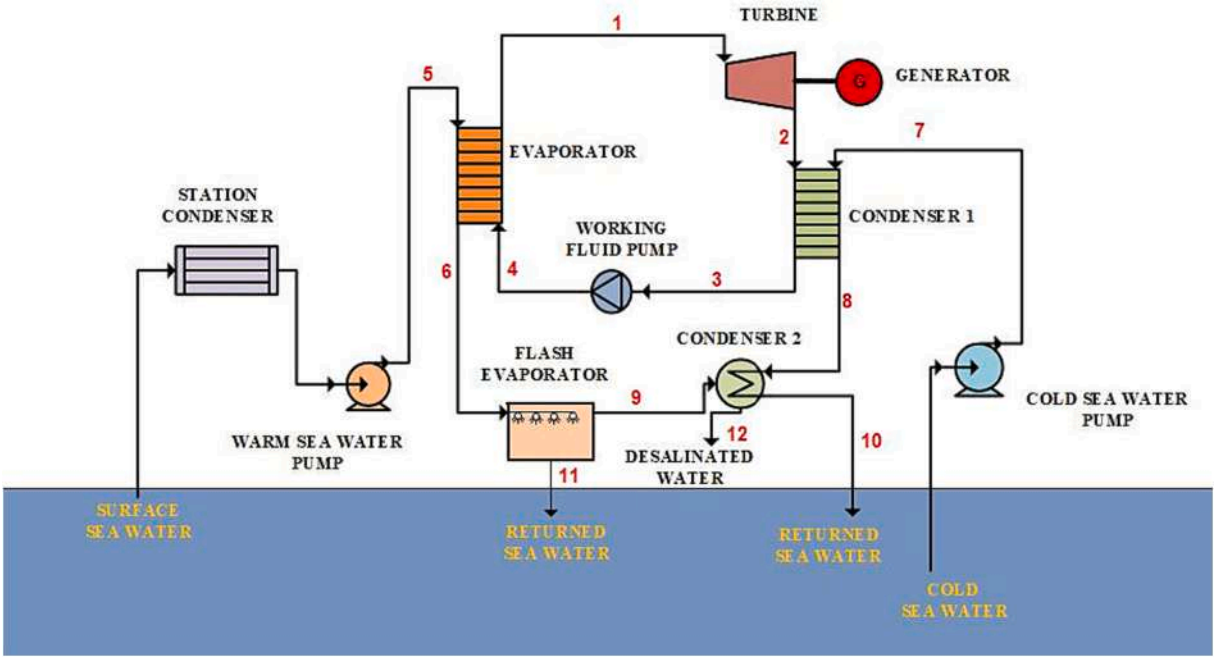


**Fig. 1.** Schematic of the OTEC basic cycle using the condenser outlet water of a thermal power plant [5].

then the exergy rate of each component are calculated. An exergy analysis for the basic cycle will also be performed. In the following, the proposed cycle and the available relationships for analyzing various components of the cycle are introduced.

Fig. 2 shows the schematic of the proposed OTEC combined cycle, which uses a two-stage turbine with reheating and warm water output from the thermal power plant condenser. This cycle can be divided into two parts: power generation and freshwater production. In order to improve the performance of an OTEC cycle, the turbine in the basic cycle will be replaced by a two-stage turbine with a reheating stage. An extraction path with an open type heater (which is actually a direct contact heater) has also been used. In addition to, a close-type heater will be used to increase the temperature of the working fluid. The power generation section consists of a closed Rankine cycle with ammonia as

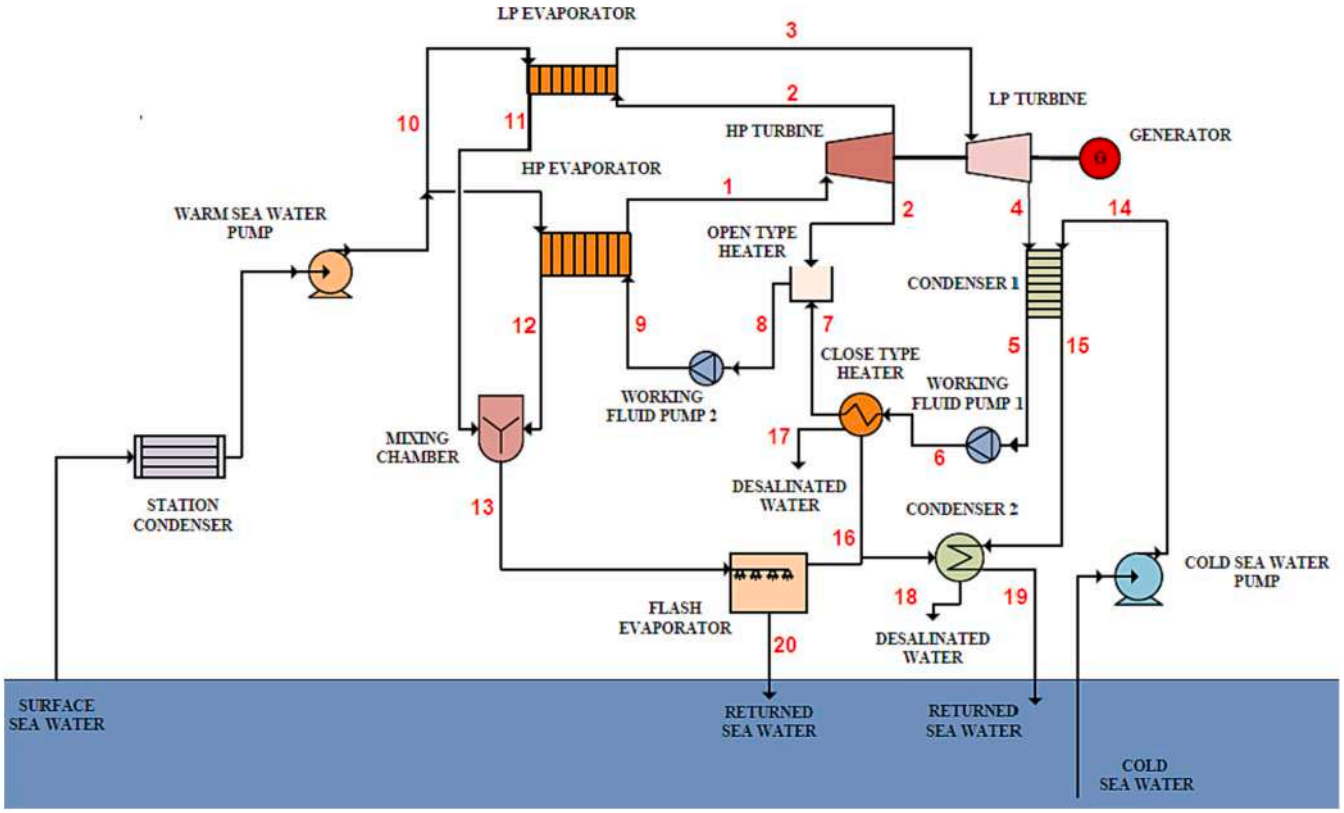


**Fig. 2.** Schematic of the proposed OTEC cycle using the outlet water of the thermal power plant condenser.

the working fluid, where the power generated by the turbine is used to run the generator and finally generate electricity. The warm water leaving the condenser of the thermal power plant enters the Rankine cycle's evaporators through the warm seawater pump. Most warm seawater enters the high pressure (HP) evaporator and leaves it after transferring heat to ammonia. The saturated ammonia vapor enters the high-pressure turbine and, after turning to medium pressure, will enter the low-pressure evaporator. This ammonia vapor becomes superheated at constant pressure and enters the LP turbine by absorbing thermal energy from the rest of the warm seawater in the low-pressure evaporator. This part of the ammonia vapor leaves the turbine after generating power and enters the main condenser. In the ammonia condenser, heat transfer is carried out with cold water coming from the depths of the sea to the condenser by a cold seawater pump. After condensation in the saturated liquid state, it is compressed again by fluid pump number 1 to the middle pressure. After passing through the heater, it closes and enters the open type heater after increasing its temperature. In the open type heater, it is combined with the extracted vapor from the HP turbine. Finally, in the saturated liquid state at the pressure of the heater, it enters pump II and then sent back to the HP evaporator, where the cycle gets closed.

The second part of the cycle is related to freshwater production, which includes a mixing chamber to combine the two warm water streams leaving the evaporators, the flash evaporator to produce water vapor, and a condenser to condense the vapor produced in the flash evaporator. In this section, first, the seawater streams enter the mixing chamber after leaving the Rankine cycle evaporators and are combined directly. This warm water flow enters the flash evaporator after leaving the mixing chamber. The internal pressure is kept lower than atmospheric pressure by a vacuum pump, and part of the inlet seawater evaporates into the flash evaporator due to pressure reduction. Part of this produced water vapor enters the close-type heater, and after transferring heat to the liquid ammonia, it leaves the close-type heater as a liquid. The main part of the produced vapor also enters the desalination condenser and does heat transfer to cold water in the deep part of the sea, which comes from the main condenser of the Rankine cycle. Finally, the vapor leaves the condenser after condensing and producing freshwater. Finally, the warm seawater that has not been evaporated in the flash evaporator is discharged to the sea at a lower temperature. In this way, the environmental problems caused by the discharge of warm water from the condenser will also be alleviated.

In the following, the available relationships associated with modeling and thermodynamic analysis of different components of the cycle will be introduced.

## 3. Energy and exergy analysis

### 3.1. Energy analysis

One of the first laws of thermodynamics is the law of conservation of energy or the first law of thermodynamics. In the energy analysis of thermodynamic cycles, each component of the cycle is considered a control volume and the relationships related to energy conservation for each control volume is applied independently [44]:

$$\sum_{in} \dot{m}_{in} h_{in} - \sum_{out} \dot{m}_{out} h_{out} - \dot{W} + \dot{Q} = 0 \tag{1}$$

$$\sum_{i} \left( \dot{m}_{in} - \dot{m}_{out} \right) = 0 \tag{2}$$

in which, ṁ, h, Ẇ, and Q̇ stand for mass flow rate (kg/s), specific enthalpy (kJ/kg), work (kW), and heat transfer (kW), respectively.

#### 3.1.1. Problem hypotheses in energy analysis

The hypotheses considered in the energy analysis section are as follows [5]:

1. The system is considered to be steady-state.
2. Heat loss in pipes and other equipment is ignored.
3. The ammonia side pressure drop in the Rankine cycle is neglected.
4. Ammonia vapor at the inlet to the turbine is considered to be saturated vapor.
5. Ammonia in pumps is considered to be in the saturated liquid state.
6. The frictional pressure drop of the seawater pipe, the mixing chamber, and the flash evaporator are ignored.

### 3.2. Cycle component analysis

In this section, the various components of the cycle will be examined according to the equations and hypotheses mentioned.

#### 3.2.1. Operator

The evaporators used in the Rankine cycle are of the plate type and are made of titanium. Some of the design parameters of the plates have been shown in Table 1 [5].

The heat transfer rate in evaporators is obtained from Eqs. (3) and (4).

$$\dot{Q}_{EHP} = \dot{m}_{WF}.(h_1 - h_9) = \dot{m}_{WHP}.C_P.(T_{10} - T_{12}) \tag{3}$$

$$\dot{Q}_{ELP} = \left( \dot{m}_{WF} - mf_{ex} \right).(h_3 - h_2) = \dot{m}_{WLP}.C_P.(T_{10} - T_{11}) \tag{4}$$

where ($\dot{Q}_{EHP}$) represents the rate of heat transfer performed in the HP evaporator, ($\dot{Q}_{ELP}$) is the amount of heat transfer performed in the LP evaporator and ($C_P$) denotes specific heat at constant seawater pressure [5]. Also, the heat transfer rate required in evaporators will be obtained from Eqs. (5) and (6).

$$A_{EHP} = \frac{\dot{Q}_{EHP}}{U_E.\Delta T_{m.EHP}} \tag{5}$$

$$A_{ELP} = \frac{\dot{Q}_{ELP}}{U_E.\Delta T_{m.ELP}} \tag{6}$$

where, ($A_{EHP}$) represents the level required in the HP evaporator, ($\Delta T_{m.EHP}$) denotes the logarithmic mean temperature difference in the HP evaporator, ($A_{ELP}$) is the level required in LP evaporator and ($\Delta T_{m.ELP}$) is the logarithmic mean temperature differences in the LP evaporator.

#### 3.2.2. Condenser

The condenser used in the Rankine cycle is of the plate type and is made of titanium. Some of the design parameters of the plates have been shown in Table 2 [5].

The amount of heat transfer done in the condenser is obtained from Eq. (7).

$$\dot{Q}_C = \left( \dot{m}_{WF} - mf_{ex} \right).(h_4 - h_5) = \dot{m}_C.C_P.(T_{15} - T_{14}) \tag{7}$$

where ($\dot{m}_C$) is the mass flow rate of deep-sea cold water and ($C_P$) represents specific heat at constant sea cold water pressure [4]. Also, the heat transfer level required in the condenser will be obtained from Eq.

**Table 1**
Specifications of evaporator plate [5].

| Design parameter | Value | Unit |
|---|---|---|
| Overall heat transfer coefficient ($U_E$) | 4.9 | $kW.m^{-2}.K^{-1}$ |
| Effective area of the plates | 3.2 | $m^2$ |
| Spacing between plates | 5 | mm |
| Plate thickness | 1 | mm |

**Table 2**
Specification of the condenser plates [5].

| Design parameter | Value | Unit |
|---|---|---|
| Overall heat transfer coefficient ($U_C$) | 4.24 | $kW.m^{-2}.K^{-1}$ |
| Effective area of the plates | 3.2 | $m^2$ |
| Spacing between plates | 5 | mm |
| Plate thickness | 1 | mm |
| Condenser efficiency ($\in_C$) | 0.9 | – |

(8) [32].

$$A_C = \frac{\dot{Q}_C}{U_C.\Delta T_{m.C}} \tag{8}$$

where ($A_C$) represents the required level in the condenser and ($\Delta T_{m.C}$) is the logarithmic mean temperature difference in the condenser.

### 3.2.3. Working fluid pump

The consumed power of ammonia pumps is calculated by determining the working fluid flow rate and fluid enthalpy at the inlet and outlet of each pump from Eqs. (9) and (10) [5].

$$\dot{W}_{WFP1} = \frac{\left(\dot{m}_{WF} - mf_{ex}\right).(h_6 - h_5)}{\eta_{WFP1}} \tag{9}$$

$$\dot{W}_{WFP2} = \frac{\dot{m}_{WF}.(h_9 - h_8)}{\eta_{WFP2}} \tag{10}$$

where, ($\dot{W}_{WFP}$) is the consumed power of each pump and ($\eta_{WFP}$) is the efficiency of each pump, which is considered to be 0.8.

### 3.2.4. Close type heater

In order to use part of the thermal energy in the water steam produced in the flash evaporator, which is completely lost in the basic cycle, a close type heater will be used in the proposed cycle. In this heater, which is the first factor in the fluid pump outlet, the steam entering the heater is condensed after transferring heat with ammonia liquid, which is at a lower temperature than water vapor, and ammonia entering at a higher temperature will enter the open type heater.

The rate of heat transfer done in the close type heater as well as the required area of the heater will be obtained from relations (11) and (12).

$$\dot{Q}_{cth} = \dot{m}_{17}.(h_{16} - h_{17}) \tag{11}$$

$$A_{cth} = \frac{\dot{Q}_{cth}}{U_{cth}.\Delta T_{m.cth}} \tag{12}$$

where, ($\dot{Q}_{cth}$) represents the rate of heat transfer performed in the close type heater, ($\Delta T_{m.cth}$) is the logarithmic mean temperature difference in the close type heater and ($A_{cth}$) the required area in the close type heater. It should be noted that the material and specifications of the close type heater plates have been considered similar to the evaporator plates.

### 3.2.5. Open type heater

An open type heater will be used to transfer direct heat between the ammonia steam extracted in the HP turbine and the ammonia liquid leaving the close type heater. The purpose of using an open type heater is to increase the temperature of the ammonia entering the HP evaporator in the proposed cycle. The amount of extracted steam required is obtained by writing the energy balance for the open type heater according to Eq. (13).

$$mf_{ex}.h_2 + \left(\dot{m}_{WF} - mf_{ex}\right).h_7 = \dot{m}_{WF}.h_8 \tag{13}$$

### 3.2.6. Cold seawater pump

Eq. (14) is used to calculate the consumption power of the cold seawater pump [5].

$$\dot{W}_{CP} = \frac{\dot{m}_C.\Delta P_{CP}}{\eta_{CP}.\rho_C} \tag{14}$$

where ($\dot{W}_{CP}$) represents the consumed power of the cold seawater pump, ($\dot{m}_C$) is the mass flow rate of cold water, ($\rho_C$) denotes the density of cold water, ($\eta_{CP}$) pump efficiency equals to 0.8, and ($\Delta P_{CP}$) is the pressure drop in cold water section which is obtained from the sum of the friction pressure drop of the pipe, the pressure drop in the condenser and also the pressure drop due to the density difference, which will be discussed as following.

### 3.2.7. Warm seawater pump

Eq. (15) is used to calculate the consumed power of the seawater pump [5].

$$\dot{W}_{WP} = \frac{\dot{m}_W.\Delta P_{WP}}{\eta_{WP}.\rho_W} \tag{15}$$

where ($\dot{W}_{WP}$) represents the consumption power of warm sea water pump, ($\dot{m}_W$) is mass flow rate of warm water, ($\rho_W$) denotes the density of warm water, ($\eta_{WP}$) is pump efficiency equal to 0.8, and ($\Delta P_{WP}$) pressure drop in warm water part that due to the short length of the warm water pipe and also the suction of seawater from the condenser outlet of the thermal power plant.

### 3.2.8. Vacuum pump

As mentioned, the internal pressure of the flash evaporator to evaporate the inlet warm water must be lower than the saturated pressure of the incoming water at that temperature to convert part of the entering water into vapor. The internal pressure of the flash evaporator is kept constant by a vacuum pump at a constant value of 1.5 kPa for all months of the year. This pressure is lower than the saturation pressure of the coldest month of the year [5]. Eq. (16) is used to calculate the consumed power of the vacuum pump.

$$\dot{W}_{VP} = \frac{P_{ad}}{\eta_{vp}} \tag{16}$$

where, ($\dot{W}_{VP}$) denotes the consumed power of the vacuum pump, ($P_{ad}$) is the power required to discharge non-condensing gases, and ($\eta_{vp}$) represents the efficiency of the vacuum pump and is equal to 0.75.

### 3.2.9. Mixing chamber

Given that in the proposed cycle the warm water flow through the evaporators has been considered as a parallel flow, for direct mixing of these two currents passing through the evaporators, a mixing chamber has been placed before the flash evaporator in the cycle. The warm water output of each evaporator enters this mixing chamber and after a direct combination of the two currents, it leaves the chamber and then enters the flash evaporator. The temperature of the seawater at the outlet of the mixing chamber will be obtained by writing the energy balance for the chamber according to Eq. (17).

$$\dot{m}_{WLP}.h_{11} + \dot{m}_{WHP}.h_{12} = \dot{m}_W.h_{13} \tag{17}$$

### 3.2.10. Thermal efficiency

The thermal efficiency of the cycle is defined as the ratio of the useful work of the output to the input thermal energy in the evaporators and is calculated from Eq. (18) [5].

$$\eta_P = \frac{\dot{W}_{net}}{\dot{Q}_{EHP} + \dot{Q}_{ELP}} = \frac{\dot{W}_G - \dot{W}_{WFP1} - \dot{W}_{WFP2} - \dot{W}_{CP} - \dot{W}_{WP} - \dot{W}_{VP}}{\dot{Q}_{EHP} + \dot{Q}_{ELP}} \tag{18}$$

### 3.3. Exergy analysis

Exergy analysis or the second law is to justify and describe different energy flows and also to help reduce the drops that occur in a system. The exergy of a substance is divided into four components: physical, chemical, kinetic, and potential. Physical exergy is the maximum axial work that can be received from an energy stream in a set of ideal machines. Chemical exergy is also the maximum amount of work that can be extracted when the material reaches the dead state from its original state by the processes involving heat transfer and material transfer. Chemical exergy shows its importance in chemical combustion processes [45].

#### 3.3.1. Equations governing exergy analysis

The governing equations in this section for each control volume include the exergy balance equation, which is shown in Eqs. (19) to (24) [46].

$$\dot{E}_{X^Q} + \sum_i \dot{m}_{in} ex_{in} = \sum_e \dot{m}_{out} ex_{out} + \dot{E}_{X^w} + \dot{I} \tag{19}$$

$$\dot{E}_{X^Q} = \left(1 - \frac{T_0}{T_{in}}\right) \dot{Q}_i \tag{20}$$

$$ex = ex_{ph} + ex_{ch} \tag{21}$$

$$ex_{ph} = (h - h_0) - T_0(s - s_0) \tag{22}$$

$$ex_{ch} = \sum_{i=1}^{n} ex_i ex_{ch_i} + RT_0 \sum_{i=1}^{n} ex_i ln ex_i \tag{23}$$

$$\dot{E}_{X^w} = \dot{W} \tag{24}$$

where ($\dot{E}_{X^Q}$) represents the exergy of heat transfer, ($ex_{ph}$) is the physical exergy, ($ex_{ch}$) denotes the chemical exergy of mixed gases, ($\dot{E}_{X^w}$) is the exergy of work, and ($\dot{I}$) is the exergy destruction of process. Index (0) also represents the reference conditions of the environment [47–50].

#### 3.3.2. Problem hypotheses in exergy analysis

The hypotheses considered in the exergy analysis section are as follows:

1. The system is analyzed under the steady-state condition.
2. Changes in kinetic exergies and potentials can be ignored.
3. Due to the absence of chemical reactions in the system and also a slight change in the salt concentration in the freshwater production process, chemical exergy can be neglected.
4. The reference conditions of the environment are considered as the temperature of 25 degrees Celsius and the pressure of 1 atm.
5. Given the low-temperature range of seawater in the cycle and also the existence of a temperature limit ($T > 10\ ^\circ C$) to calculate seawater exergy directly in the EES software and articles related to seawater properties, thermodynamic properties related to pure water direction Exergy calculations are used in seawater.

#### 3.3.3. Exergy analysis of cycle components

In this section, according to the mentioned equations and hypotheses, the exergy balance is written for different components of the cycle and the exergy destruction in different parts of the cycle is calculated. The relationships used in this section have is shown in Table 3.

In the relationships listed in Table 1, ($E_{10HPE}$) represents the exergy of warm water flow passing through the HP evaporator, ($E_{10LPE}$) is the exergy of warm water flow passing through the LP evaporator, ($E_{2ex}$) denotes the exergy of extracted ammonia vapor, ($E_{16cth}$) is the exergy of inlet water vapor of the close-type heater, ($E_{16DC}$) represents the exergy of input water vapor of the desalinator condenser, ($E_{Ci}$) represents the exergy of cold sea water at inlet to cold water pump, ($\Delta H_{CP}$) is the head related to cold water pump, ($E_{Wi}$) denotes the exergy of warm water inlet of the warm water pump and ($\Delta H_{WP}$) is the head related to the warm water pump.

**Table 3**
The relationships used to analyze the proposed cycle exergy.

| Components | Exergy destruction rate |
|---|---|
| HP evaporator | $\dot{I}_{HPE} = (E_9 + E_{10HPE}) - (E_1 + E_{12})$ |
| LP evaporator | $\dot{I}_{LPE} = (E_{2LPE} + E_{10LPE}) - (E_3 + E_{11})$ |
| HP turbine | $\dot{I}_{HPT} = (E_1 - E_{2LPE} + E_{2ex}) - \dot{W}_{HPT}$ |
| LP turbine | $\dot{I}_{LPT} = (E_3 - E_4) - \dot{W}_{LPT}$ |
| Generator | $\dot{I}_G = (1 - \eta_G)\left(\dot{W}_{LPT} + \dot{W}_{HPT}\right)$ |
| Rankine cycle condenser | $\dot{I}_C = (E_4 + E_{14}) - (E_5 + E_{15})$ |
| Working fluid pump 1 | $\dot{I}_{WFP1} = (E_5 - E_6) + \dot{W}_{WFP1}$ |
| Working fluid pump 2 | $\dot{I}_{WFP2} = (E_8 - E_9) + \dot{W}_{WFP2}$ |
| Open-type heater | $\dot{I}_{oth} = (E_7 + E_{2ex}) - E_8$ |
| Close-type heater | $\dot{I}_{cth} = (E_6 + E_{16cth}) - (E_7 + E_{17})$ |
| Mixing chamber | $\dot{I}_{MCH} = (E_{11} + E_{12}) - E_{13}$ |
| Flash evaporator | $\dot{I}_{FE} = E_{13} - (E_{16} + E_{20})$ |
| Desalination condenser | $\dot{I}_{DC} = (E_{15} + E_{16DC}) - (E_{18} + E_{19})$ |
| Cold seawater pump [58] | $\dot{I}_{CP} = (E_{Ci} + E_{14}) + \dot{W}_{CP}$ <br> $\dot{I}_{CP} = \dot{m}_{CP}.\left[\frac{(T_0 + 273.15).q_{Ci}.\Delta H_{CP}.\left(1 + \frac{1}{\eta_{CP}}\right)}{T_{Ci} + 273.15}\right]$ |
| Hot seawater pump [58] | $\dot{I}_{WP} = (E_{Wi} + E_{10}) + \dot{W}_{WP}$ <br> $\dot{I}_{WP} = \dot{m}_{WP}.\left[\frac{(T_0 + 273.15)q_{Wi}.\Delta H_{WP}\left(1 + \frac{1}{\eta_{WP}}\right)}{T_{Wi} + 273.15}\right]$ |
| Output exergy of the cycle | $\dot{I}_{loss} = E_{17} + E_{18} + E_{19} + E_{20}$ |

#### 3.3.4. Exergy efficiency

Total exergy efficiency is defined as the ratio of useful output work to input exergy and is calculated from Eq. (25).

$$\eta_{ex} = \frac{\dot{W}_{net}}{\dot{E}_{Xin}} \tag{25}$$

Input exergy into the cycle is the sum of warm and cold seawater exergies as well as inlet exergy into the system due to the operation of working fluid pumps, which is calculated from Eq. (26).

$$\dot{E}_{Xin} = \dot{E}_{X10} + \dot{E}_{X14} + \dot{W}_{WFP1} + \dot{W}_{WFP2} \tag{26}$$

### 3.4. Validation

To validate the modeling performed in the energy analysis section, the results obtained by Soto and Vergara [5] were used, and the parameters of output power, thermal efficiency and fresh water production in the modeling performed with the results of the main cycle is compared and the degree of agreement of the results is examined. The thermodynamic parameters of different points of the basic cycle for March as an example have been shown in Table 4.

#### 3.4.1. Cycle output power validation

The output power of the main cycle for different months of 2010 provided by Soto and Vergara [5] is shown by the modeling results of the present study with Fig. 3a and b that the comparison of the results shows a good agreement in the results.

#### 3.4.2. Thermal efficiency validation

The thermal efficiency of the main cycle for different months of 2010 presented by [5] with the modeling results of the present study is shown in Fig. 4, where the comparison of the results shows a significant agreement.

**Table 4**
Thermodynamic parameters of different points of the basic cycle in March.

| Points | Temperature (°C) | Pressure (kPa) | Mass flow rate (kg/s) | Specific enthalpy (kJ/kg) | Specific entropy (kJ/kg-K) | Quality |
|---|---|---|---|---|---|---|
| 1 | | | | | | |
| 2 | 8.80 | 590.2 | 668.8 | 1425 | 5.35 | 0.963 |
| 3 | 8.80 | 590.2 | 668.8 | 240.9 | 1.15 | 0 |
| 4 | 8.92 | 988.1 | 668.8 | 241.7 | 1.15 | 0 |
| 5 | 27.50 | 107.7 | 26,208 | 109.8 | 0.38 | 0 |
| 6 | 19.59 | 101.3 | 26,208 | 78.29 | 0.28 | 0 |
| 7 | 5.80 | 131.1 | 73,400 | 27.41 | 0.09 | 0 |

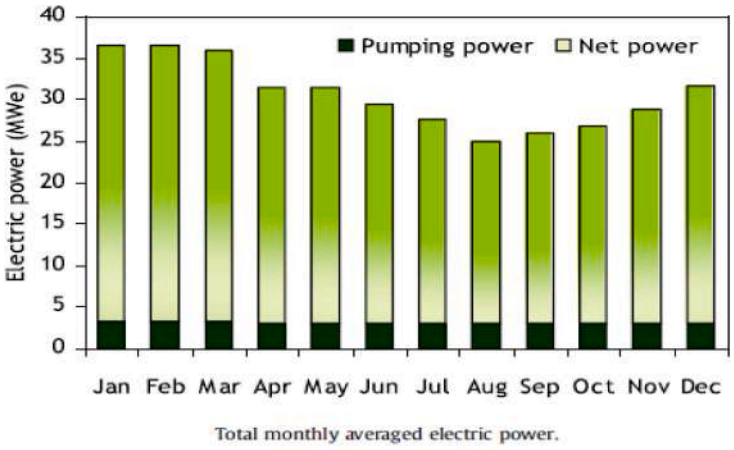


a. Output power and net monthly production power of Soto and Vergara study [5]

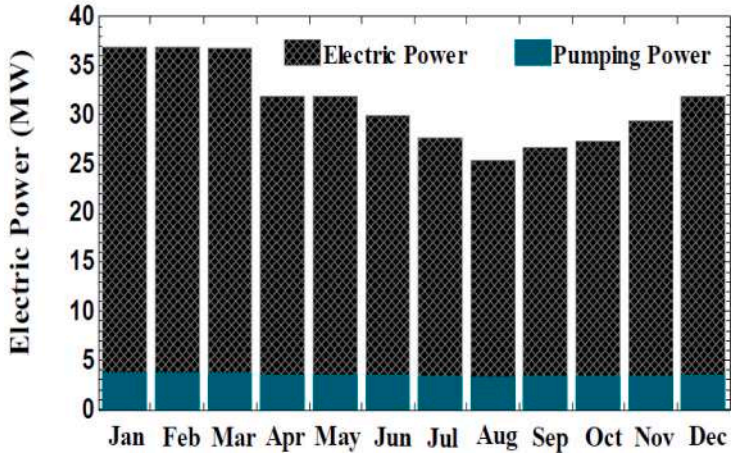


b. Output power and monthly production power of the present study

**Fig. 3.** a. Output power and net monthly production power of Soto and Vergara study [5].
b. Output power and monthly production power of the present study.

## 4. Result and discussion

As mentioned above, in the OTEC basic cycle proposed by Soto and Vergara, a 740 MW condenser output warm water in Chile was used instead of surface warm water to increase the efficiency and output power of the OTEC cycle. In this section, at first, this cycle will be modeled by the EES software, the exergy analysis provided by Soto and Vergara cycles [5] will be performed. In the following, the results of the energy and exergy modeling of the new proposed cycle is presented and compared with the basic cycle parameters and the results will be reviewed and analyzed.

### 4.1. Exergy analysis of the basic cycle

In the basic cycle, only energy analysis was done by Soto and Vergara [5] and the results were presented. In this section, as a new analysis, first, the basic cycle is modeled in terms of exergy and after presenting the results, in the next section, the results are compared to the simulation results of the proposed cycle.

#### 4.1.1. Basic cycle exergy efficiency

As mentioned, exergy efficiency is defined as the ratio of net power output to input exergy into the cycle. Fig. 5 shows the monthly exergy efficiency for the basic cycle. As shown in this figure, the highest exergy

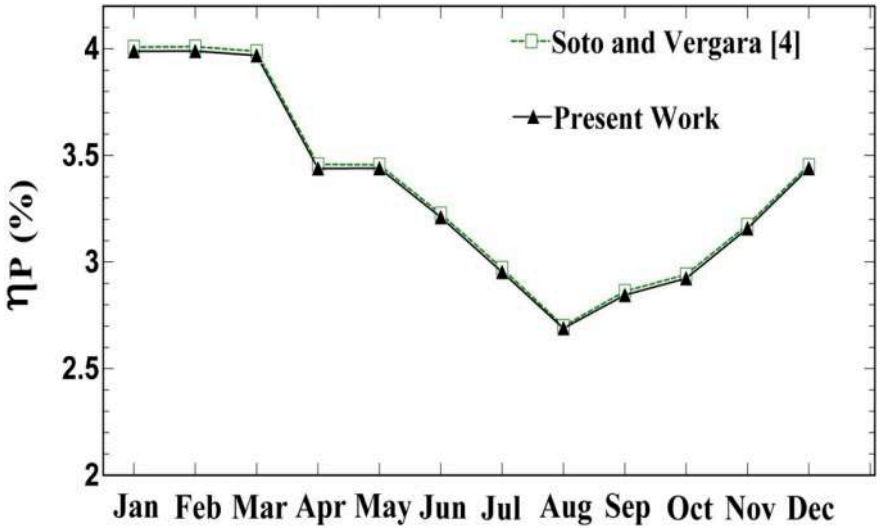


**Fig. 4.** Monthly thermal efficiency of Soto and Vergara study and present study [5].

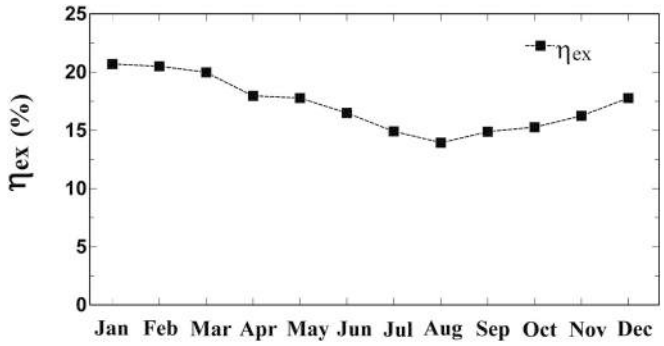


**Fig. 5.** Monthly exergy efficiency of the basic cycle.

efficiency was obtained in January at 20.69 % and the lowest exergy efficiency was associated with August at 13.94 %. Monthly changes in exergy also indicate that in months when the temperature difference between surface warm water and cold sea water is greater, the exergy efficiency will have a higher number than the thermal efficiency of the cycle. This is due to the electrical power production in the cycle in these months.

#### 4.1.2. Input exergy and exergy destruction

As mentioned, the exergy input of the cycle is equal to the sum of the exergies of cold and warm seawater, as well as the exergy input of the system due to the operation of the working fluid pump. Seawater exergy depends on the difference between the water temperature and the reference temperature, and the greater the temperature difference, the higher the seawater exergy. As shown in Fig. 6, in July and March, the exergy input of the cycle has the highest value, due to the greater temperature difference between the cold water temperature of the deep sea and the reference temperature in those months. The highest exergy destruction is related to July and August because of the high exergy loss through the seawater outlet in those months.

#### 4.1.3. Exergy destruction of components

One of the goals of exergy analysis in any system is to determine the share of components in the exergy destruction of the whole system in order to identify the most inefficient component with the highest rate of exergy destruction so to improve its performance. Therefore, the exergy destruction percentage of each component is determined from the exergy destruction of all components. As an example, the results associated with the month of March are shown in Fig. 5. As shown in Fig. 7, the flash evaporator and desalination condenser with a share of 31.77 % and 30.46 %, respectively, had the highest share of exergy destruction

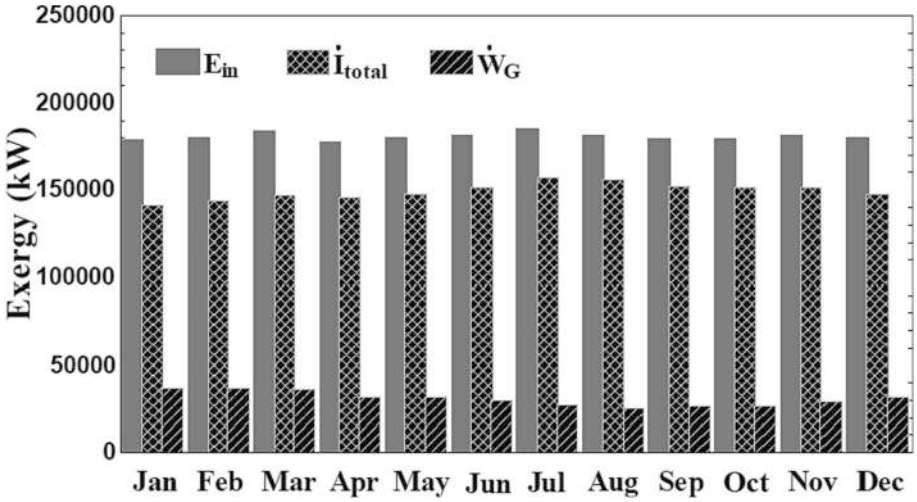


**Fig. 6.** Monthly Input exergy and exergy destruction rates in the basic cycle.

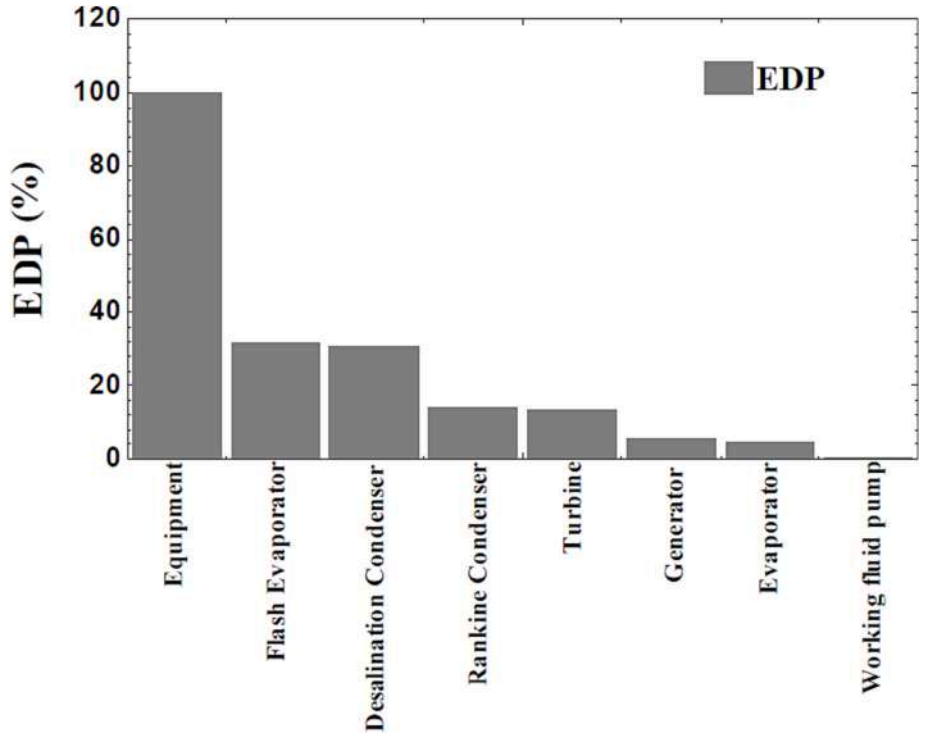


**Fig. 7.** Exergy destruction percentage of different components of the basic cycle in March.

among all components, which is due to the phenomenon of flushing and vacuum vapor production in the flash evaporator and also the temperature and pressure difference between warm and cold flows and the desalination condenser. In the third and fourth places are Rankine condenser and turbine cycle, with 14.08 and 13.32 %, respectively.

*4.1.4. Exergy efficiency of components*

In this section, the exergy efficiency of each component is determined, defined as the ratio of the optimal exergy produced to the exergy used in each component. Again, the results for March are presented as an example in Fig. 8. As is shown, among all components, the flash evaporator and desalination condenser, with 33.71 and 62.09 %, respectively, have the lowest exergy efficiency. This is due to the higher exergy destruction rates in these two components. Also, the highest exergy efficiency was related to the generators and turbines, with 95 % and 89.49 %, respectively.

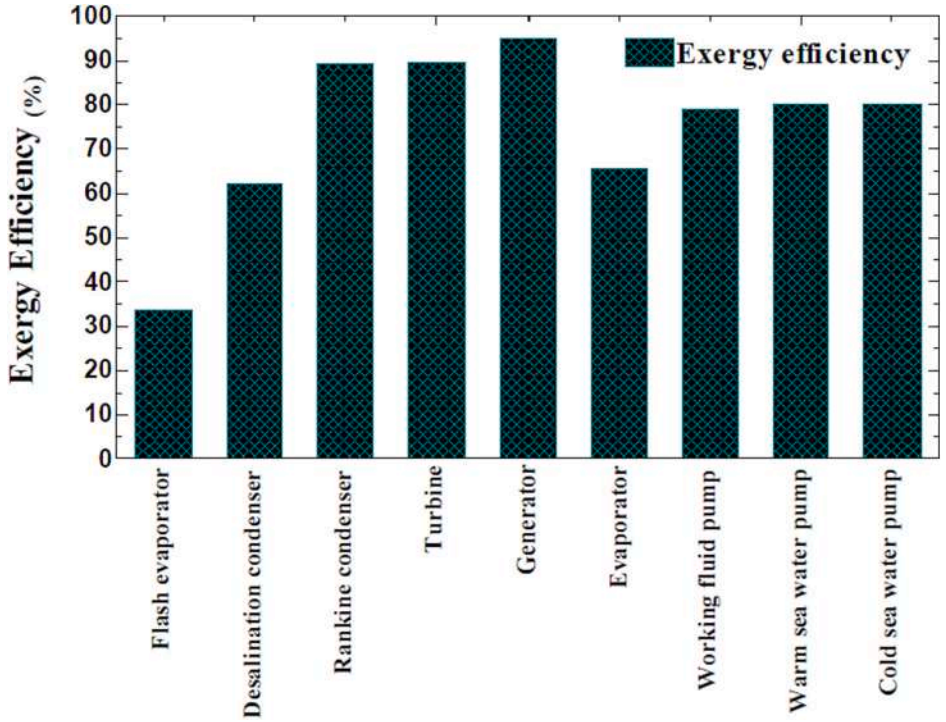


**Fig. 8.** Exergy efficiency of different components of the basic cycle in March.

#### 4.1.5. Exergy diagram

An exergy diagram, also known as a Grassmann diagram, is used to quantify exergy currents in a thermodynamic system or cycle. Fig. 9 shows the Grassmann diagram in March for the basic cycle. As can be seen from the figure, out of 183,780 kW of input exergy into the cycle in March, 36,720 kW (equivalent to 19.98 % of the input exergy into the cycle) is removed as electrical power, and the rest as exergy destruction is wasted in the cycle. The largest share of exergy destruction is related to the loss of exergy through the outflow of warm and cold sea water as well as freshwater produced in the cycle, equal to 112,964 kW (61.48 %). Also, 344,096 kW (18.54 %) is also destructed in the cycle components. Overall, as also mentioned in the previous section, the flash evaporator with 10,831 kW of exergy destruction (5.89 %) has the largest share in the total exergy destruction rate.

### 4.2. Energy analysis of the novel proposed cycle

In this section, the proposed novel cycle is modeled and analyzed from the perspective of energy and exergy, and then the results will be compared to that of the basic cycle to evaluate the benefits of the new cycle. To analyze the energy of the proposed cycle, the same general equations and hypotheses are implemented in the EES software.

It is necessary to mention that in the proposed cycle, the correct range of some parameters such as pressure ratio in the HP turbine, mass flow ratio in The LP evaporator, the temperature difference between ammonia output from the LP evaporator and warm water inlet to the LP evaporator, etc. are determined and used in the coding process. However, these parameters can be optimized in future research to optimize the overall performance of the proposed cycle. The thermodynamic parameters of different points of the proposed cycle for March is shown in Table 5 and the T-S diagram of the power generation of the OTEC cycle including an organic Rankine cycle (ORC) with ammonia working fluid is drawn for the month of March are shown in Fig. 10.

#### 4.2.1. Generated electrical power

A comparison of the electrical power generation of the proposed cycle with the basic cycle is shown in Fig. 11. According to the results, the output power in the proposed cycle is increased for all months compared to the basic cycle, varying from 720 kWh in January to 407 kWh in August. On average, the output power increases by 552 kWh per month compared to the basic cycle [5].

Fig. 12 also compares the net monthly output power of the proposed cycle and the basic cycle, where the increase in net output power produced by the proposed cycle for all months is evident. This increase in net power varies from 709 kWh in January to 398 kWh in August. When compared to the basic cycle, the average increase is 543 kWh per month [5].

#### 4.2.2. Thermal efficiency

A comparison of the thermal efficiency of the proposed cycle with the basic cycle is shown in Fig. 13. As it is clear from the results, the thermal efficiency in the new cycle for all months has increased due to the increase in output power in the cycle and also the implementation of heaters. This increase in efficiency varies from 0.062 % in March to 0.035 % in August and it shows an average thermal efficiency increase of 0.048 % per month compared to the basic cycle [5].

#### 4.2.3. Vapor quality at the turbine outlet

The presence of liquid particles in the vapor causes corrosion and damage to the turbine blades, where it is most evident in end blades with larger areas. The quality of vapor output from the turbine is one of the important parameters in the safe operation of the turbine. One way to increase the quality of the turbine output is to use multi-stage turbines with reheating. Considering the use of two-stage turbines with reheating in the proposed cycle, while improving the performance parameters of the basic cycle, the vapor quality at the output of the HP and LP turbines also increases compared to the basic cycle. This reduces corrosion and

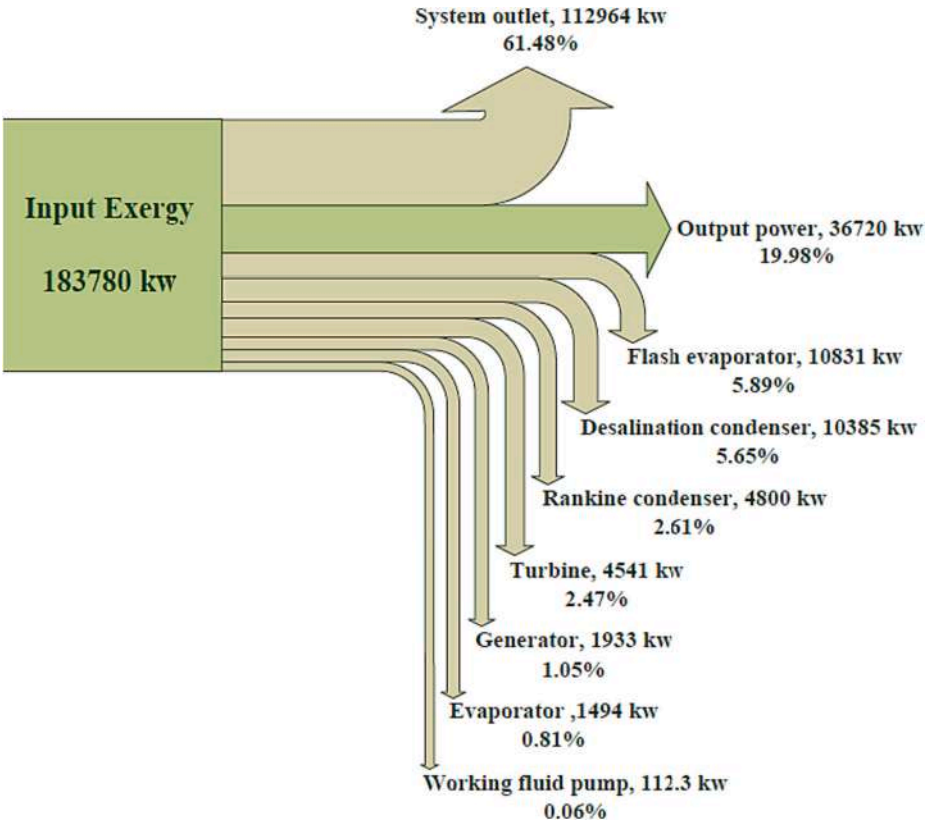


**Fig. 9.** Grassmann diagram for the basic cycle in March.

**Table 5**
Thermodynamic parameters points of the proposed cycle in March.

| Points | Substance | Temperature (°C) | Pressure (kPa) | Mass flow rate (kg/s) | Specific enthalpy (kJ/kg) | Specific entropy (kJ/kg-K) | Quality |
|---|---|---|---|---|---|---|---|
| 1 | Ammonia | 24.5 | 988.1 | 672.5 | 1483 | 5.32 | 1 |
| 2 | Ammonia | 18.03 | 805.1 | 656.68 | 1460 | 5.33 | 0.98 |
| 2ex | Ammonia | 18.03 | 805.1 | 15.82 | 1460 | 5.33 | 0.98 |
| 3 | Ammonia | 26.5 | 805.1 | 656.68 | 1503 | 5.48 | 1 |
| 4 | Ammonia | 8.8 | 590.2 | 656.68 | 1467 | 5.49 | 0.99 |
| 5 | Ammonia | 8.8 | 590.2 | 656.68 | 240.9 | 1.14 | 0 |
| 6 | Ammonia | 8.87 | 805.1 | 656.68 | 241.4 | 1.15 | 0 |
| 7 | Ammonia | 12.02 | 805.1 | 656.68 | 256.1 | 1.20 | 0 |
| 8 | Ammonia | 18.03 | 805.1 | 672.5 | 284.4 | 1.30 | 0 |
| 9 | Ammonia | 18.09 | 988.1 | 672.5 | 284.8 | 1.31 | 0 |
| 10 | Seawater | 27.5 | 107.7 | 26,208 | 109.8 | 0.38 | 0 |
| 11 | Seawater | 22.05 | 101.3 | 1310 | 88.08 | 0.31 | 0 |
| 12 | Seawater | 19.42 | 101.3 | 24,898 | 77.6 | 0.27 | 0 |
| 13 | Seawater | 19.55 | 101.3 | 26,208 | 78.13 | 0.28 | 0 |
| 14 | Seawater | 5.8 | 131.1 | 73,400 | 27.41 | 0.09 | 0 |
| 15 | Seawater | 8.545 | 126.8 | 73,400 | 38.38 | 0.13 | 0 |
| 16 | Steam | 13.02 | 1.5 | 286.9 | 2524 | 8.83 | 1 |
| 17 | Freshwater | 13.02 | 1.5 | 3.924 | 54.64 | 0.20 | 0 |
| 18 | Freshwater | 13.02 | 1.5 | 283 | 54.64 | 0.20 | 0 |
| 19 | Seawater | 10.93 | 126.8 | 73,400 | 47.91 | 0.16 | 0 |
| 20 | Seawater | 13.02 | 1.5 | 25,921 | 52.13 | 0.19 | 0 |

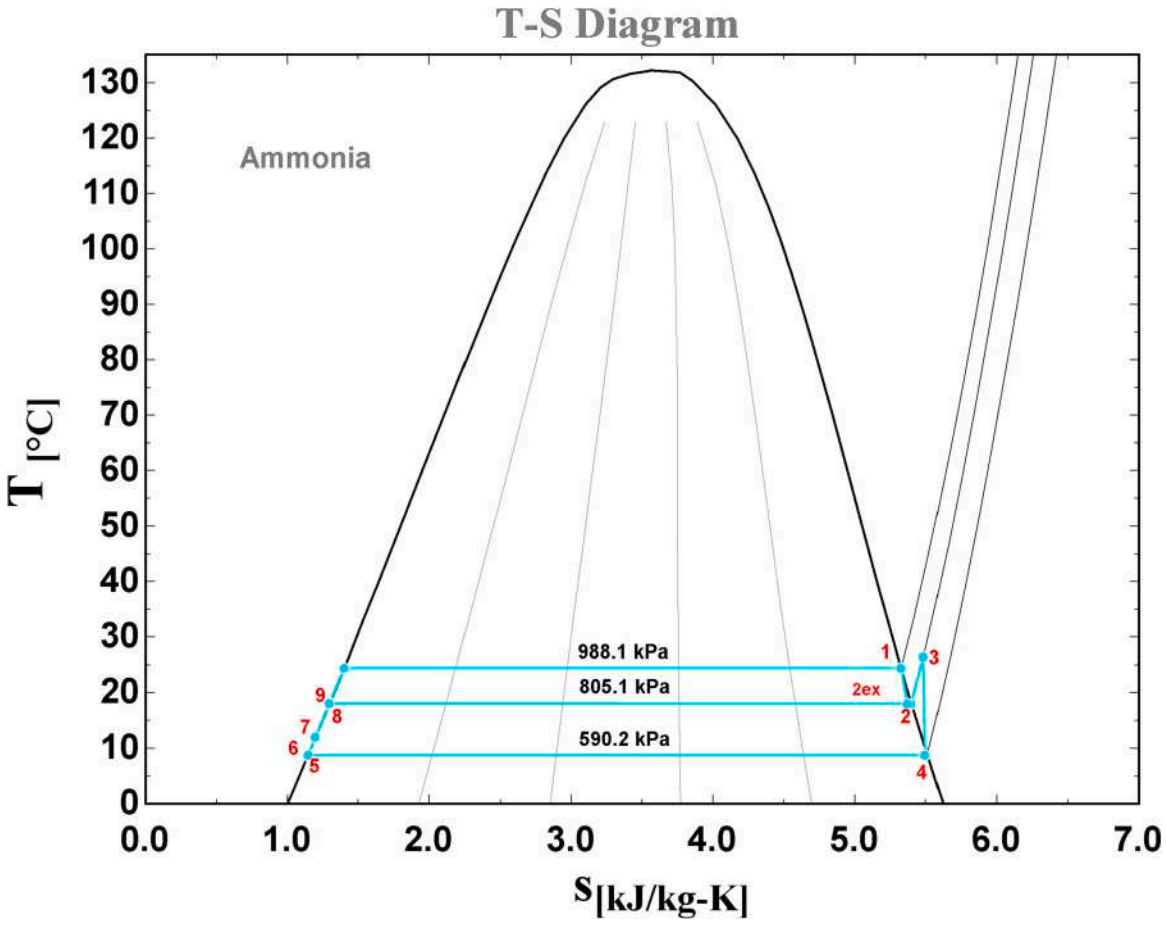


**Fig. 10.** T-S diagram of different points of the proposed cycle in March.

enhances the performance of the turbine. As shown in Fig. 14, the quality of vapor output from the turbine in the proposed cycle is in much better condition than the basic cycle.

*4.2.4. Fresh water production*

The fresh water production rate in the proposed cycle and the basic cycle are shown in Fig. 15. As can be seen, the freshwater production rate in the proposed cycle is decreased slightly in all months due to the decrease in the temperature of the water entering the flash evaporator. Reducing the inlet water temperature to the flash evaporator reduces the superheat degree difference causes a smaller amount of water input of the flash evaporator due to reduced pressure, and ultimately reduces the fresh water production rate in the proposed cycle. This decrease in the freshwater production rate varies from 219 tons per day in January to

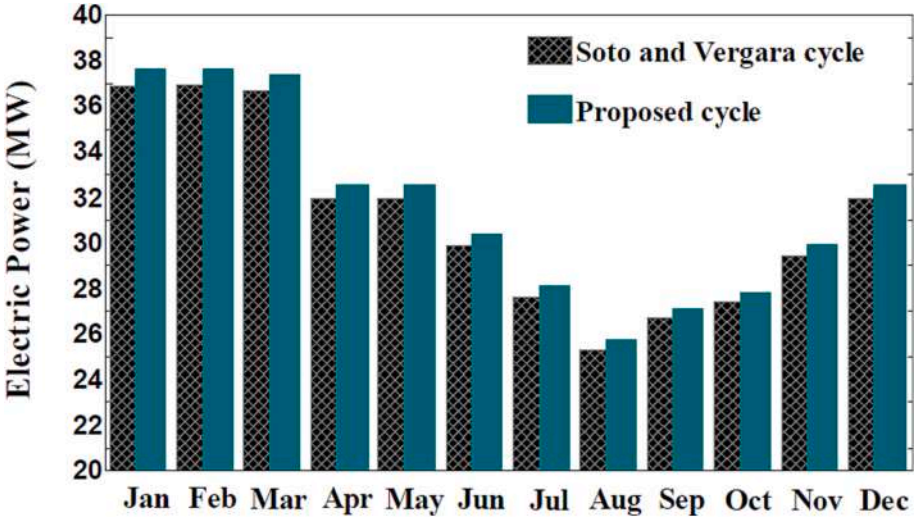


**Fig. 11.** Comparison of the electric generating power of the proposed cycle and the basic cycle.

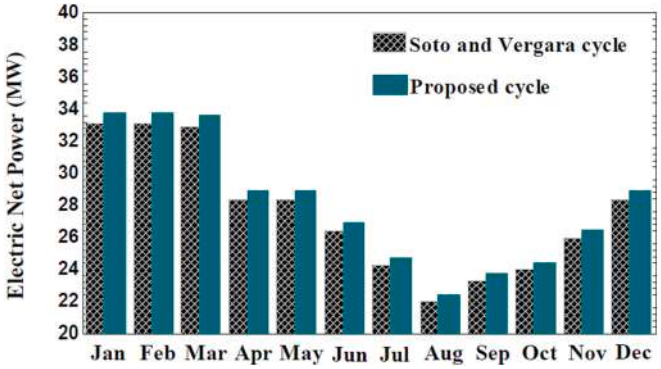


**Fig. 12.** Comparison of the electrical net output power of the proposed cycle and the basic cycle.

132 tons per day in July. On average, the freshwater production rate in the proposed cycle decreases by 175 tons per day per month compared to the basic cycle (equivalent to a decrease of 1.09 %) [5].

### *4.3. Exergy analysis of the new proposed cycle*

In this section, the exergy analysis of the proposed cycle is performed using the equations and hypotheses mentioned before, the results of which and their comparison with the basic cycle will be explained as follows.

#### *4.3.1. Total exergy destruction*

As for similarities between the 2 cycles, the temperature conditions are the same, which also holds true for the mass flow rate of warm and cold sea water. The only difference between the exergy input and output is due to the small differences in the total consumed power of the working fluid pumps. Therefore, the input exergy to both cycles can be considered approximately equal in different months. The rate of total exergy destruction in the proposed cycle and the basic cycle is shown in Fig. 16. According to the figure, for all months, the total exergy destruction in the proposed cycle is reduced compared to the basic cycle. Part of this reduction is due to the destruction of exergy in the component and partly due to the increase in output power. It is worth mentioning that since the exergy input of the cycle is not changed significantly compared to the basic cycle, this leads to a decrease in the exergy destruction of the entire proposed cycle.

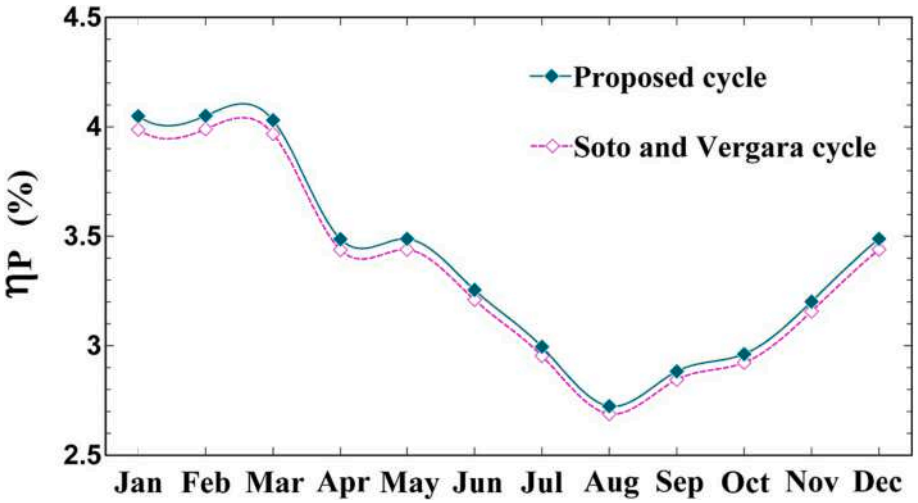


**Fig. 13.** Comparison of the thermal efficiency of the proposed cycle and the basic cycle.

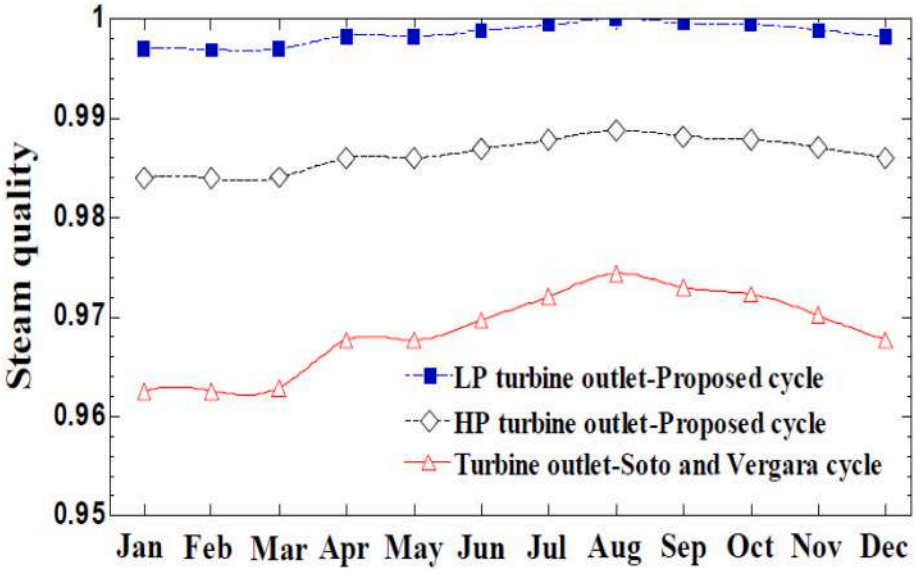


**Fig. 14.** Comparison of turbine output vapor quality in the proposed cycle and the basic cycle.

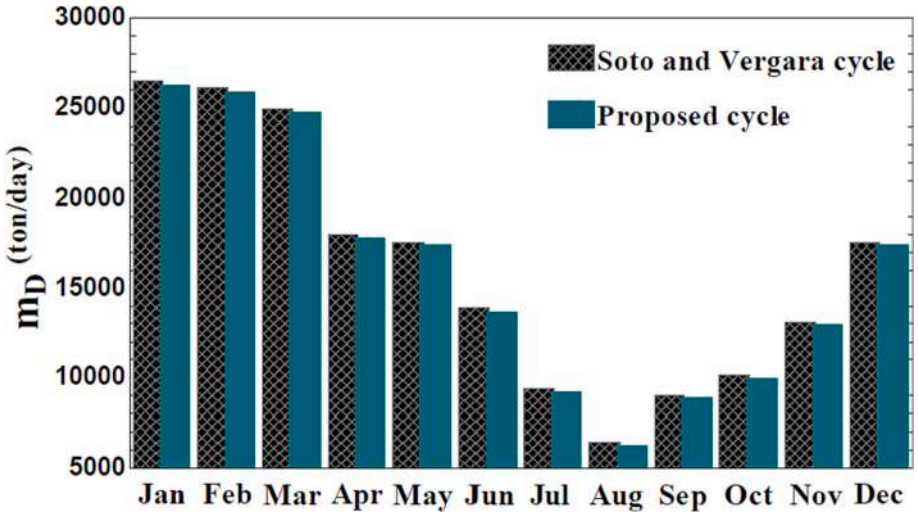


**Fig. 15.** Comparison of fresh water production rate in the proposed cycle and the basic cycle.

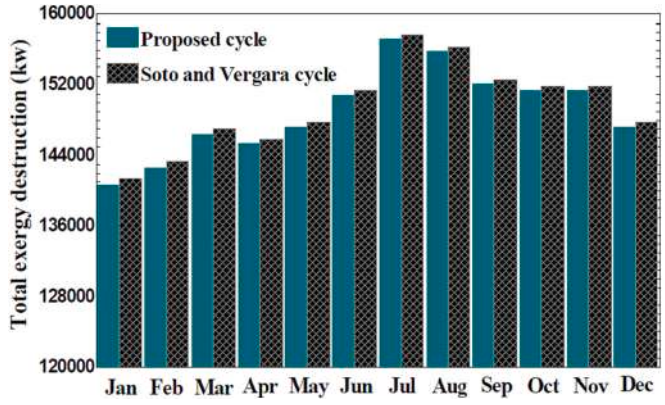


**Fig. 16.** Comparison of total exergy destruction in the proposed cycle and the basic cycle.

*4.3.2. Exergy efficiency*

A comparison of the exergy efficiency of the proposed cycle with the basic cycle is exhibited in Fig. 17. As it is clear from the results, given the

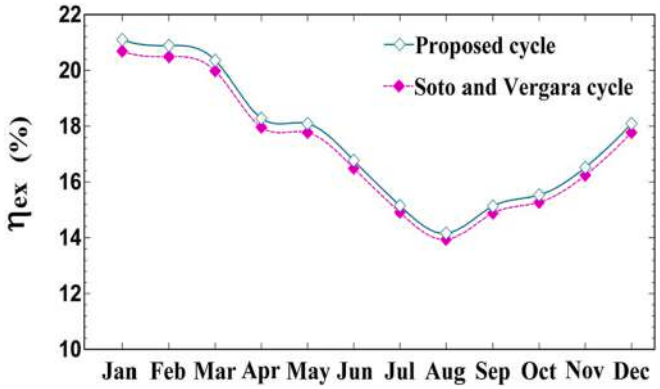


**Fig. 17.** Comparison of exergy efficiency in the proposed cycle and the basic cycle.

uniformity of the input exergy into the cycle, due to the increase in output power and also the reduction of the total exergy destruction in the proposed cycle, the exergy efficiency in the proposed cycle has increased for all months compared to the basic cycle. This increase in efficiency varies from 0.41 % in January to 0.22 % in August and it also shows an average exergy efficiency of 0.31 % per month compared to the basic cycle.

#### 4.3.3. Exergy destruction of components

Computed for March, the exergy destruction percentage of each component is determined from the exergy destruction of all components and shown in Fig. 15. The exergy destruction rate of all components in March for the basic cycle was 34,096 kW. This is reduced to 33,314 kW in the proposed cycle, and the exergy destruction rate of components is reduced to 782 kW. As shown in Fig. 18, similar to the basic cycle, the flash evaporator and desalination condenser, with 32.1 % and 30.36 % of the total component exergy destruction in this month, respectively, have the highest shares of exergy destruction in all components. They are followed by two other components: The Rankine cycle's condenser and LP turbine, with 14.41 % and 8.34 %, respectively.

#### 4.3.4. Exergy efficiency of components

Similar to the basic cycle, the exergy efficiency of the proposed cycle's components is determined and results for March are given in Fig. 19. As is shown, among the components, an open type heater and mixing chamber have the highest exergy efficiency due to both low exergy destruction and direct mixing of the input streams in them. Also, similar to the basic cycle, despite the increase in exergy efficiency in the flash evaporator and desalination condenser, with 34.6 and 62.4 %, respectively, they have the lowest exergy efficiency among other components. The only decrease in exergy efficiency among the proposed cycle's components compared to that of the basic cycle is related to the evaporator, considering the fact that parameters such as the expansion ratio of turbines and the mass flow rate of warm water passing through evaporators have not been optimized in this study. By achieving the optimal values of the abovementioned parameters, the reduction of efficiency in the evaporator can also be corrected.

#### 4.3.5. Exergy diagram

Similar to the basic cycle, the exergy diagram in March for the proposed cycle is plotted in Fig. 20. According to the figure, out of the total 183,781 kW of input exergy in March, 37,417 kW (20.36 %) is removed to produce electrical power and the rest is lost in the form of exergy destruction. Similar to the basic cycle, the largest share of exergy destruction is related to the loss of exergy through the outflow of warm and cold seawater as well as fresh water produced in the cycle, which is equal to 113,050 kW (61.53 %). Also, 33,314 kW (equivalent to 18.11 %) is also destructed in the cycle equipment.

Among the cycle components, as mentioned in the previous section, the flash evaporator has the largest share in the total exergy destruction. Despite the reduction of 137 kW in the exergy destruction compared to the basic cycle, with 10,694 kW (5.82 %), the flash evaporator has the highest contribution.

## 5. Case study of CCPP

In the previous sections, modeling of the basic cycle and the proposed cycle were performed and the results were compared from two perspectives of energy and exergy. The results showed an improvement in the performance of the new cycle compared to the basic cycle. In this section, for a case study, the proposed cycle has been modeled using the data of the Shahid Salimi combined cycle power plant (CCPP), which is located on the Caspian Sea coast, north of Iran, and the results will be extracted and examined, which will be discussed below.

### 5.1. Introduction of CCPP

This Power Plant is one of the most important national assets and one of the largest power plants in the country. This power plant consists of two independent heating and combined cycle parts and is located on the Caspian Sea coast in Iran. The nominal power of this power plant is 2214 MW, which consists of four steam units each with a nominal power of 440 MW, a combined cycle block consisting of two gas turbine units each with a nominal power of 137.6 MW, and a steam unit with a nominal power of 160 MW and also two turbo expander units with a nominal power of 9.4 MW.

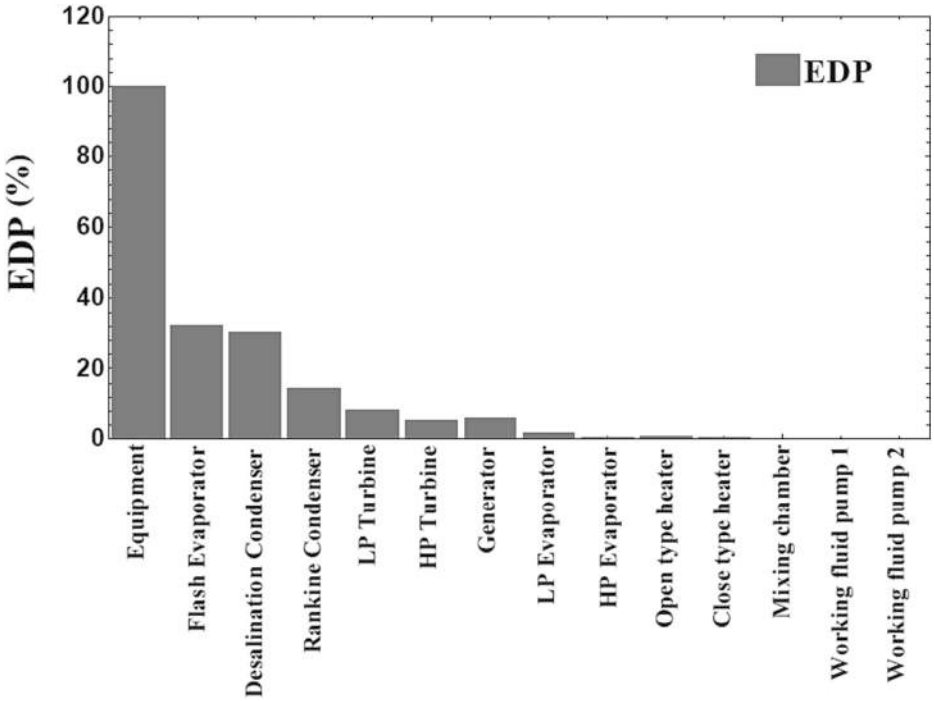


**Fig. 18.** Exergy destruction percentage of different components of the proposed cycle in March.

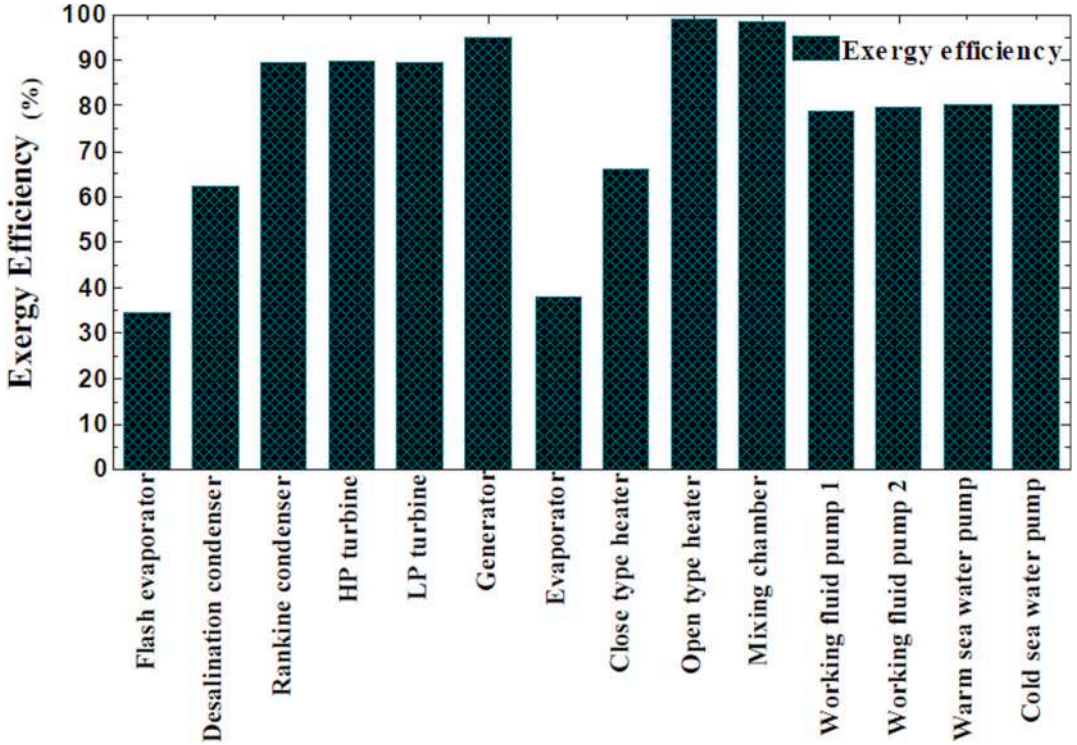


**Fig. 19.** Exergy efficiencies of the various components of the proposed cycle in March.

The Heat Recovery Steam Generator (HRSG) used in the CCPP is of the two-pressure drum type with auxiliary burners that are used to supply the steam required for the steam turbine. Given the fact that this power plant is located on the shores of the Caspian Sea, the Caspian Sea water is used for the cooling system related to the condenser. Seawater is sent to the condenser by two axial flow pumps with a volume flow of approximately 39,000 cubic meters per hour, and after the steam condenses, this water is discharged back into the sea at a high temperature. The condenser design of CCPP is such that the sea water is heated to 10 °C after passing through the condenser and absorbing the heat of the steam coming out of the turbine, which discharges this high volume of warm water back to the sea in addition to high energy loss.

### 5.2. Generated electrical power

The electricity production rate, pump consumed power and net monthly power output have been shown in Fig. 21. As can be seen from the figure, given that the proposed basic cycle has been presented by Soto and Vergara in Chile, located in the Southern Hemisphere, the results of a case study at the CCPP have been inverted due to its location in the Northern Hemisphere. For example, in the basic cycle, output power had the highest value in February and the lowest value in August, which in the case study has been reversed [5]. According to the modeling results, the generated electric power varies from 29.8 MWh in July to 11.3 MWh in February, and on average, each month, the proposed cycle will generate an electrical power of 20.2 MWh using warm water from the condenser of CCPP. The consumed power of the pumps varies from 2.7 MWh in July to 2.2 MWh in February and the average consumed power of the pumps is 2.48 MWh. Considering the generated electric power, the average net generating power of the cycle will be 17.72 MWh per month.

### 5.3. Thermal efficiency

Monthly thermal efficiency values are shown in Fig. 22. As shown in the figure, due to the high surface water temperature entering the condenser of CCPP, compared to the surface water temperature of the Pacific Ocean used in the proposed cycle, the temperature difference created in the cycle increased leading to an increase in the thermal efficiency in a case study. Thermal efficiency varies from 7.132 % in July to 2.507 % in February and, the average monthly efficiency for the proposed cycle in the case study is 4.768 %. Therefore, in the case of using the warm water of the condenser outlet of CCPP in the proposed cycle, the average thermal efficiency compared to the average efficiency of 3.336 % in the basic cycle provided by Soto and Vergara has increased by 1.432 %, which is equivalent to 42.93 % improvement in thermal efficiency of Soto and Vergara cycles [5].

### 5.4. Exergy efficiency

Monthly exergy efficiency values are shown in Fig. 23. Similar to the thermal efficiency described in the previous section, due to the increase in temperature difference in the cycle. Also, due to the lower mass flow rate of warm and cold seawater compared to the basic cycle, the input exergy of the cycle has decreased significantly. For example, in the basic cycle, the maximum input exergy of the cycle in July was 185,328 kW, while the maximum input exergy in the case study decreased again in July to 93,389 kW. According to the mentioned explanations, the exergy efficiency in the proposed cycle for the case study has significantly increased compared to the basic cycle. Exergy efficiency varied from 31.91 % in July to 16.21 % in February and the average monthly exergy efficiency for the proposed cycle in the case study is 25.22 %. Therefore, if the condenser output warm water of CCPP is used in the proposed cycle, the average exergy efficiency compared to the average efficiency of 17.2 % in the basic cycle has increased by 8.02 %, which is equivalent to 46.63 % improvement in Exergy efficiency is the basis of Soto and Vergara cycles.

### 5.5. Fresh water production

The monthly freshwater production rate is shown in Fig. 24. The freshwater production rate varies from 33,004 tons per day in July to 3645 tons per day in February. On average, the proposed cycle using the

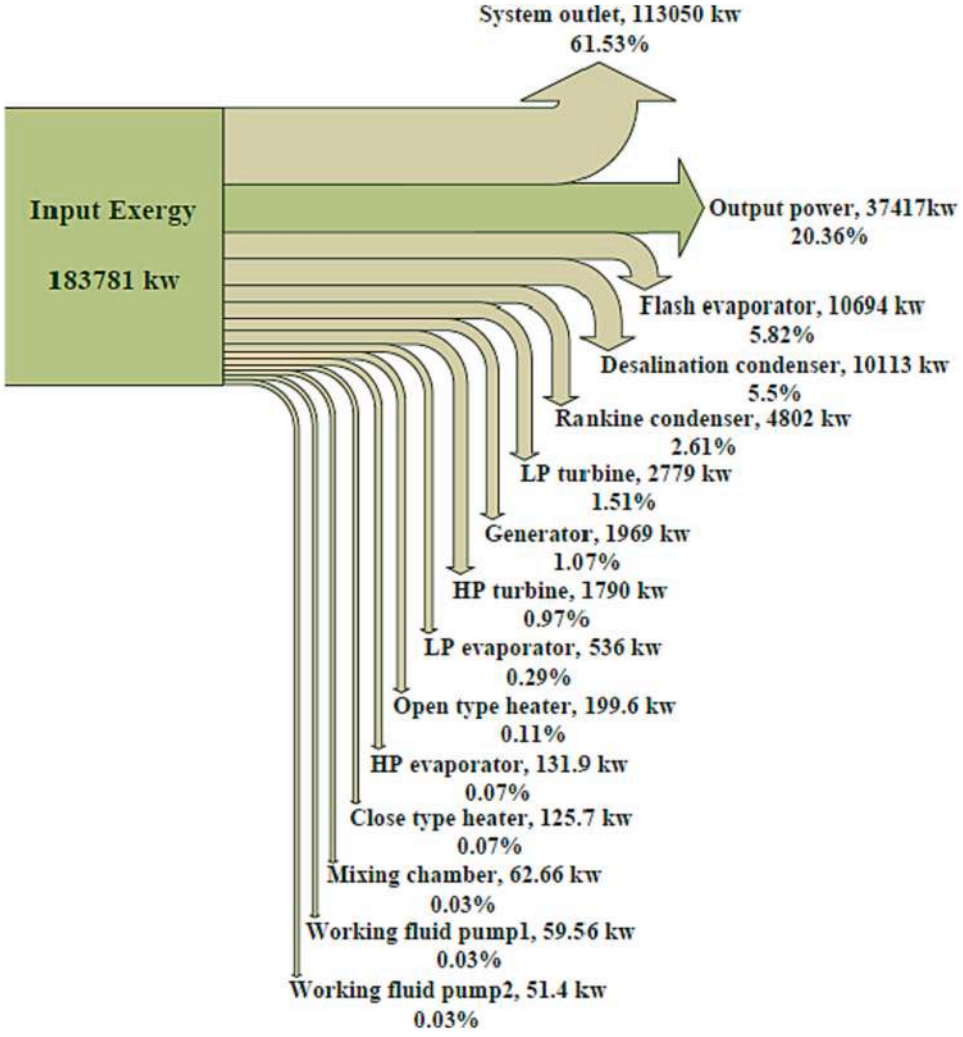


**Fig. 20.** Grassmann diagram for the proposed cycle in March.

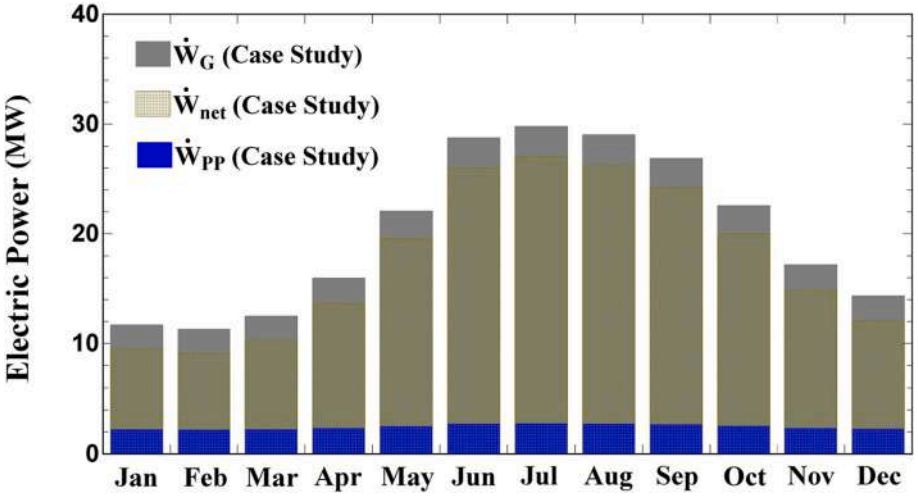


**Fig. 21.** Electric generating power, pump consumed power and net monthly produced power of the OTEC cycle proposed in the case study.

warm water output from the condenser of CCPP has the ability to produce 18,829 tons of fresh water per day per month. Using this high volume of freshwater produced in the proposed cycle, in addition to eliminating the need for water consumption of the entire power plant, including four steam units and also a combined cycle unit, the surplus sale of fresh water produced can also be a significant source of revenue for the power plant. Using this volume of fresh water produced, the need to use chemical units in the power plant to produce fresh water also

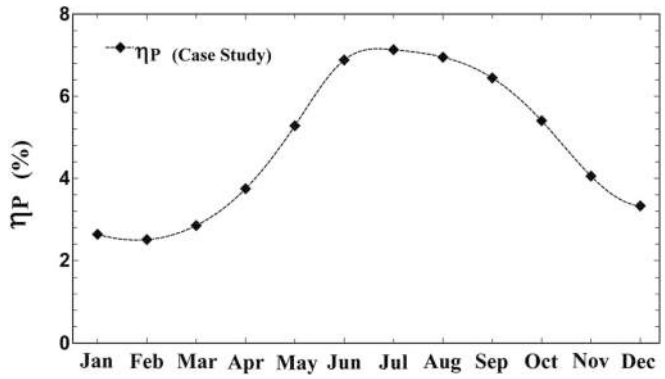


**Fig. 22.** The monthly thermal efficiency of the OTEC cycle proposed in the case study.

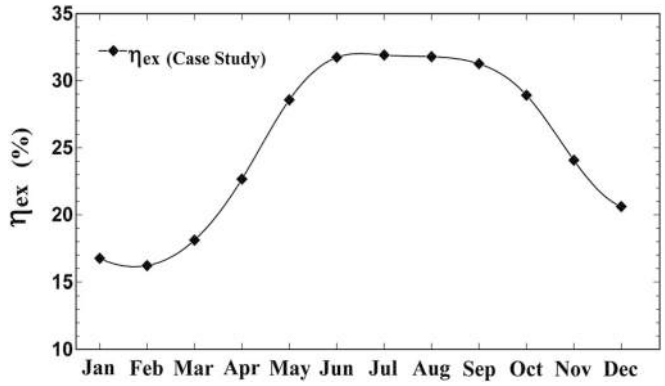


**Fig. 23.** Monthly exergy efficiency of the proposed OTEC cycle in a case study.

imposes high costs on the power plant. It will also eliminate the use of wells currently used to supply raw water to chemical units. A comparison of freshwater production rate in a case study with the Soto and Vergara basic cycles shows that although the water outflow rate from the combined cycle condenser is much lower than the basic cycle. However, due to the high sea surface temperature in the CCPP, which increases the temperature of the inlet water to the flash evaporator chamber, a higher percentage of inlet seawater evaporates to the flash evaporator chamber and finally more fresh water is produced in the case study. To better understand the effect of surface water temperature on freshwater production rate, it should be noted that the average freshwater production rate in the basic cycle of Soto and Vergara was 16,044 tons per day, which is only equal to 0.7 % of the total warm water inlet of the flash evaporator [5]. In the case study in CCPP, this value is 18,829 tons per day, which is equivalent to 2.1 % of the total water inlet of the flash evaporator.

### 5.6. Improvement of efficiency of CCPP

As mentioned in the previous sections, one of the purposes of using the warm water of the thermal power plant condenser outlet in the OTEC combined cycle is to increase the efficiency of the main thermal power plant presented by Soto and Vergara [5]. According to the results presented in the previous sections, it was found that the net generating capacity of the cycle in the case study varied from 27.024 MWh in July to 9.121 MWh in February and the average net generated power was 17.72 MWh per month. Considering that the output power of CCPP is equal to 435 MW and its average efficiency is 45.82 %, as a result of using the condenser outlet water of CCPP in the proposed cycle, the cycle efficiency will be increased from 2.847 % in July to 0.961 % in February. On average, using the proposed cycle in CCPP, the thermal efficiency of this power plant will be improved by 1.87 %. This increase in efficiency indicates a higher efficiency improvement compared to the 1.3 % value provided by Soto and Vergara for the coal-fired power plant in Chile [5].

## 6. Conclusion

In this study, modeling of the basic cycle and the proposed cycle were performed and the results were compared from two perspectives of energy and exergy. In the proposed cycle, in addition to using the warm water of the condenser outlet of the thermal power plant, two high-pressure and low-pressure turbines with a reheating stage between the turbine stages have been used. Also, in the proposed cycle, an extraction step in the HP turbine with two open and close-type heaters is used to improve the performance of the basic OTEC cycle, and the effect of these alterations on the performance of the proposed cycle was investigated and the corresponding results were compared to the basic OTEC cycle.

Using the warm water output of the thermal power plant condenser as a heat source in the OTEC cycle, in addition to increasing the thermal efficiency and improving the performance of the OTEC cycle, increased the efficiency of the main thermal power plant due to the use of heat

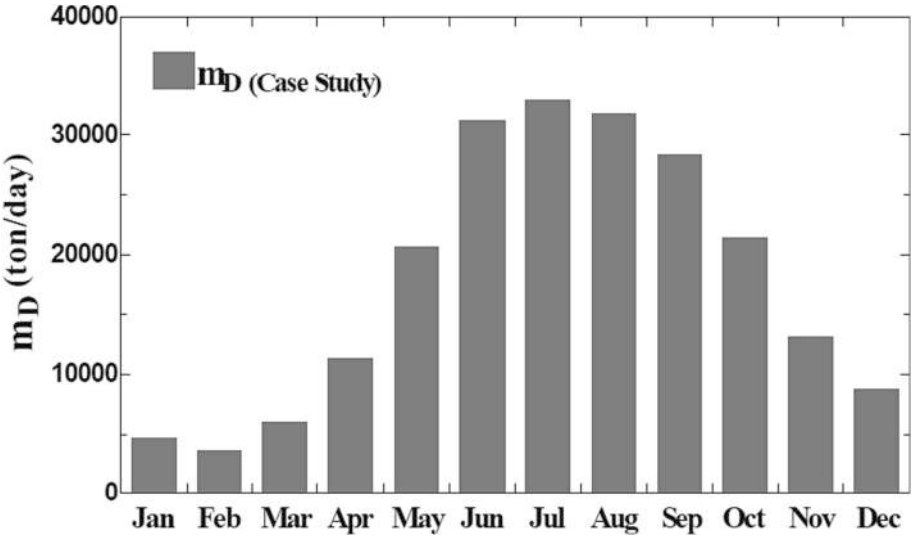


**Fig. 24.** Monthly freshwater production of the proposed OTEC cycle in a case study.

losses in the thermal power plant condenser. In the present study, the energy and exergy analysis of the basic cycle presented by Soto and Vergara was performed. Then, the new proposed cycle was presented in the form of using a two-stage turbine with reheating, as well as the use of extraction in HP turbines and open and close type heaters. For the new cycle, energy and exergy analyses were performed and the results of the proposed cycle and the basic cycle were compared.

### 6.1. Basic cycle

- The use of warm water outlet of the condenser of the thermal power plant, due to the greater temperature difference in the OTEC cycle, increases the efficiency and output power in the cycle.
- The cold sea water pump has the highest consumed power among the cycle components due to the high mass flow of cold water and also the long length of the cold water pipe, which causes more pressure drop on the cold water pipe side.
- Given the fact that Chile is located in the southern hemisphere, the highest cycle exergy efficiency was related to January, with 20.69 %. In this month, the largest temperature difference between warm surface water and cold sea water, which led to the higher electricity production rate in this month, was observed. Also, the average exergy efficiency of the cycle was 17.2 %.
- Due to the high mass flow rate of warm and cold seawater, the highest exergy destruction rate in the cycle was due to the outflow of warm and cold sea water as well as freshwater produced in the cycle, which had on average >83 % of the total exergy destruction rate.
- Among the cycle components, the flash evaporator, due to the flushing phenomenon and vacuum vapor production, and the desalination condenser, due to temperature difference and pressure of warm and cold currents with temperature and reference point pressure, had the highest exergy destruction rates. Modifying these components would improve the total performance.

### 6.2. New cycle

- Due to the changes made to the proposed cycle compared to the basic cycle, on average, the electrical power generation rate as well as net generated power increased by 552 kWh and 543 kWh, respectively.
- Thermal efficiency, due to increased output power and also the use of heaters, increased compared to the basic cycle and the average thermal efficiency improved by 0.048 %.
- The vapor quality at the output of the HP and LP turbines was significantly improved compared to the vapor quality at the output of the turbine in the basic cycle, due to the use of a two-stage turbine with reheating between the two stages. This led to the reduction of corrosion and damage to the blades and ultimately better performance of the turbine than the basic cycle.
- Due to the decrease in seawater temperature at the entrance of the flash evaporator compared to the basic cycle, which is due to the absorption of more energy from the warm seawater by the evaporators, the freshwater production rate per month decreased on average by 1.09 % compared to the basic cycle.
- Given the similarity of the input exergy of both cycles, due to the increase in output power and also the reduction of the total exergy destruction compared to the basic cycle, the average exergy efficiency increased by 0.31 % per month.
- Considering the changes made to the basic cycle, the components' exergy destruction rates in different months in the proposed cycle decreased compared to the basic cycle. In March, for example, the reduction was 782 kW.
- Similar to the basic cycle, the flash evaporator and desalination condenser had the highest percentage of exergy destruction among all components, followed by the Rankine cycle condenser and LP turbine. These can also be improved.

### 6.3. Case study

- Using the warm water output of the power plant combined cycle condenser, the proposed cycle produces an average of 17.72 MWh of net power per month.
- Due to the high surface water temperature of the Caspian Sea compared to the surface temperature of the Pacific Ocean used in the basic cycle, the average thermal efficiency of the proposed cycle is 4.768 %, which has increased by 1.432 % compared to the average efficiency of the basic cycle. This increase rate is equivalent to 42.93 % improvement in the basic cycle efficiency.
- Due to the higher temperature difference than the basic cycle, less exergy destruction and also the reduction of the input exergy into the cycle compared to the basic cycle, which is due to the lower discharge of warm and cold sea water than the basic cycle, the exergy efficiency is significantly increased compared to the basic cycle. The average exergy efficiency was 25.22 %, which increased by 8.02 % compared to the average exergy efficiency in the basic cycle. This increase is equivalent to 46.63 % improvement in the basic cycle exergy efficiency.
- Due to the higher surface water temperature of the Caspian Sea compared to the basic cycle, the temperature of the water entering the flash evaporator in the case study increased compared to the basic cycle and a higher percentage of water inlet of the flash evaporator was vapored and finally fresh water production rate increases. On average, the proposed cycle uses the power plant combined cycle condenser outlet water to produce 18,829 tons of fresh water per day, which is equivalent to 2.1 % of the total water entering the flash evaporator.
- Using the warm water output of power plant combined cycle condenser in the proposed cycle, the efficiency of power plant combined cycle will increase by an average of 1.87 %.

### 6.4. Recommendations for future work

- Optimization of parameters in the proposed cycle, including pressure ratio in the HP turbine, mass flow rate in the LP evaporator, and temperature difference between output ammonia of the LP evaporator and input warm water of the LP evaporator.
- Performing economic analysis for the proposed cycle.
- Using a solar collector to further increase the temperature of the input water and its effect on the performance of the proposed cycle.
- Investigating the effect of different working fluids on the performance of the proposed cycle.

## CRediT authorship contribution statement

**Siamak Hoseinzadeh:** Conceptualization, Data curation, Formal analysis, Funding acquisition, Investigation, Methodology, Project administration, Resources, Software, Supervision, Validation, Visualization, Writing – original draft, Writing – review & editing. **Mehdi Asadi PaeinLamouki:** Conceptualization, Data curation, Formal analysis, Investigation, Methodology, Resources, Software, Validation, Visualization, Writing – original draft. **Davide Astiaso Garcia:** Formal analysis, Investigation, Supervision, Writing – review & editing.

## Declaration of competing interest

The authors declare that they have no known competing financial interests or personal relationships that could have appeared to influence the work reported in this paper.

## Data availability

Data will be made available on request.

## References


[1] D. Gielen, F. Boshell, D. Saygin, M.D. Bazilian, N. Wagner, R. Gorini, The role of renewable energy in the global energy transformation, Energy Strateg. Rev. 24 (2019) 38–50, https://doi.org/10.1016/j.esr.2019.01.006.

[2] A. Khademi, K. Shank, S.A.A. Mehrjardi, S. Tiari, G. Sorrentino, Z. Said, A. J. Chamkha, S. Ushak, A brief review on different hybrid methods of enhancement within latent heat storage systems, J. Energy Storage 54 (2022) 105362, https://doi.org/10.1016/j.est.2022.105362.

[3] A. Mahmoudan, F. Esmaeilion, S. Hoseinzadeh, M. Soltani, P. Ahmadi, M. Rosen, A geothermal and solar-based multigeneration system integrated with a TEG unit: development, 3E analyses, and multi-objective optimization, Appl. Energy 308 (2022) 118399, https://doi.org/10.1016/j.apenergy.2021.118399.

[4] N. Arcuri, R. Bruno, P. Bevilacqua, LNG as cold heat source in OTEC systems, Ocean Eng. 104 (2015) 349–358, https://doi.org/10.1016/j.oceaneng.2015.05.030.

[5] R. Soto, J. Vergara, Thermal power plant efficiency enhancement with ocean thermal energy conversion, Appl. Therm. Eng. 62 (2014) 105–112, https://doi.org/10.1016/j.applthermaleng.2013.09.025.

[6] S. Rehman, L.M. Alhems, M.M. Alam, L. Wang, Z. Toor, A review of energy extraction from wind and ocean: technologies, merits, efficiencies, and cost, Ocean Eng. 267 (2023) 113192, https://doi.org/10.1016/j.oceaneng.2022.113192.

[7] J. Herrera, S. Sierra, A. Ibeas, Ocean thermal energy conversion and other uses of deep sea water: a review, J. Mar. Sci. Eng. 9 (2021) 356, https://doi.org/10.3390/jmse9040356.

[8] Y. Yang, Y. Wang, Z. Ma, S. Wang, A thermal engine for underwater glider driven by ocean thermal energy, Appl. Therm. Eng. 99 (2016) 455–464, https://doi.org/10.1016/j.applthermaleng.2016.01.038.

[9] K. Hall, S. Kelly, L. Henry, Site selection of ocean thermal energy conversion (OTEC) plants for Barbados, Renew. Energy 201 (2022) 60–69, https://doi.org/10.1016/j.renene.2022.11.049.

[10] C. Bernardoni, M. Binotti, A. Giostri, Techno-economic analysis of closed OTEC cycles for power generation, Renew. Energy 132 (2019) 1018–1033, https://doi.org/10.1016/j.renene.2018.08.007.

[11] M.H. Yang, R.H. Yeh, Analysis of optimization in an OTEC plant using organic Rankine cycle, Renew. Energy 68 (2014) 25–34, https://doi.org/10.1016/j.renene.2014.01.029.

[12] D.H. Johnson, Exergy of the ocean thermal resource and the second-law efficiency of idealized ocean thermal energy conversion power cycles, Energy 8 (1982) 927–946.

[13] M.H. Yang, R.H. Yeh, The investigation of optimum multi-component blends in organic Rankine cycle for ocean thermal energy conversion, Appl. Therm. Eng. 217 (2022) 119279, https://doi.org/10.1016/j.applthermaleng.2022.119279.

[14] M.H. Yang, R.H. Yeh, Investigation of the potential of R717 blends as working fluids in the organic Rankine cycle (ORC) for ocean thermal energy conversion (OTEC), Energy 245 (2022) 123317, https://doi.org/10.1016/j.energy.2022.123317.

[15] C. Li, L. Pan, Y. Wang, Thermodynamic optimization of Rankine cycle using CO2-based binary zeotropic mixture for ocean thermal energy conversion, Appl. Therm. Eng. 178 (2020) 115617, https://doi.org/10.1016/j.applthermaleng.2020.115617.

[16] H. Uehara, A. Miyara, Y. Ikegami, T. Nakaoka, Performance analysis of an OTEC plant and a desalination plant using an integrated hybrid cycle, J. Sol. Energy Eng. Trans. ASME 118 (1996) 115–122, https://doi.org/10.1115/1.2847976.

[17] K.G. Nithesh, D. Chatterjee, Numerical prediction of the performance of radial inflow turbine designed for ocean thermal energy conversion system, Appl. Energy 167 (2016) 1–16.

[18] C. Ezgi, Thermodynamic analysis of a closed-cycle ocean thermal energy conversion power plant for offshore platforms, J. Sh. Prod. Des. 38 (2022) 215–219.

[19] N. Samsuri, N. Sazali, A.S. Jamaludin, M.N.M. Razali, Techno-economic efficiencies and environmental criteria of ocean thermal energy conversion closed Rankine cycle using different working fluids, in: Proceedings of the IOP Conference Series: Materials Science and Engineering vol. 1062, IOP Publishing, 2021, p. 12042.

[20] D.-Y. Kim, Y.-T. Kim, Preliminary design and performance analysis of a radial inflow turbine for ocean thermal energy conversion, Renew. Energy 106 (2017) 255–263.

[21] S.M. Abbas, H.D.S. Alhassany, D. Vera, F. Jurado, Review of enhancement for ocean thermal energy conversion system, J. Ocean Eng. Sci. (2022), https://doi.org/10.1016/j.joes.2022.03.008.

[22] Z. Wu, H. Feng, L. Chen, Z. Xie, C. Cai, Pumping power minimization of an evaporator in ocean thermal energy conversion system based on constructal theory, Energy 181 (2019) 974–984.

[23] W. Chen, E. Huo, Opportunities and challenges of ocean thermal energy conversion technology, Front. Energy Res. (2023) 11.

[24] H. Yuan, P. Zhou, N. Mei, Performance analysis of a solar-assisted OTEC cycle for power generation and fishery cold storage refrigeration, Appl. Therm. Eng. 90 (2015) 809–819, https://doi.org/10.1016/j.applthermaleng.2015.07.072.

[25] P. Ahmadi, I. Dincer, M.A. Rosen, Energy and exergy analyses of hydrogen production via solar-boosted ocean thermal energy conversion and PEM electrolysis, Int. J. Hydrogen Energy 38 (2013) 1795–1805, https://doi.org/10.1016/j.ijhydene.2012.11.025.

[26] A. Khosravi, S. Syri, M.E.H. Assad, M. Malekan, Thermodynamic and economic analysis of a hybrid ocean thermal energy conversion/photovoltaic system with hydrogen-based energy storage system, Energy 172 (2019) 304–319, https://doi.org/10.1016/j.energy.2019.01.100.

[27] S. Khanmohammadi, M.M. Baseri, P. Ahmadi, A.A.A. Al-Rashed, M. Afrand, Proposal of a novel integrated ocean thermal energy conversion system with flat plate solar collectors and thermoelectric generators: energy, exergy and environmental analyses, J. Clean. Prod. 256 (2020) 120600, https://doi.org/10.1016/j.jclepro.2020.120600.

[28] M. Temiz, I. Dincer, A unique ocean and solar based multigenerational system with hydrogen production and thermal energy storage for Arctic communities, Energy 239 (2022) 122126, https://doi.org/10.1016/j.energy.2021.122126.

[29] F. Yilmaz, Energy, exergy and economic analyses of a novel hybrid ocean thermal energy conversion system for clean power production, Energ. Conver. Manage. 196 (2019) 557–566, https://doi.org/10.1016/j.enconman.2019.06.028.

[30] P. Ahmadi, I. Dincer, M.A. Rosen, Performance assessment of a novel solar and ocean thermal energy conversion based multigeneration system for coastal areas, J. Sol. Energy Eng. Trans. ASME 137 (2015) 11013, https://doi.org/10.1115/1.4028241.

[31] L. Wang, X. Ma, H. Kong, R. Jin, H. Zheng, Investigation of a low-pressure flash evaporation desalination system powered by ocean thermal energy, Appl. Therm. Eng. 212 (2022) 118523, https://doi.org/10.1016/j.applthermaleng.2022.118523.

[32] M.Z. Malik, F. Musharavati, S. Khanmohammadi, M.M. Baseri, P. Ahmadi, D. D. Nguyen, Ocean thermal energy conversion (OTEC) system boosted with solar energy and TEG based on exergy and exergo-environment analysis and multi-objective optimization, Sol. Energy 208 (2020) 559–572, https://doi.org/10.1016/j.solener.2020.07.049.

[33] S. Hoseinzadeh, E. Assareh, A. Riaz, M. Lee, D. Astiaso Garcia, Ocean thermal energy conversion (OTEC) system driven with solar-wind energy and thermoelectric based on thermo-economic analysis using multi-objective optimization technique, Energy Rep. 10 (2023) 2982–3000, https://doi.org/10.1016/j.egyr.2023.09.131.

[34] Y. Gao, Y. Deng, W. Yao, Y. Hang, Optimization of combined cooling, heating, and power systems for rural scenario based on a two-layer optimization model, J. Build. Eng. 60 (2022) 105217, https://doi.org/10.1016/j.jobe.2022.105217.

[35] J.Y. Jung, H.S. Lee, H.J. Kim, Y. Yoo, W.Y. Choi, H.Y. Kwak, Thermoeconomic analysis of an ocean thermal energy conversion plant, Renew. Energy 86 (2016) 1086–1094, https://doi.org/10.1016/j.renene.2015.09.031.

[36] Y. Liu, Y. Xue, Y. Chen, W. Liu, Y. Ge, L. Zhang, Identification of nonparametric thermodynamic model and optimization of ocean thermal energy conversion radial inflow turbine, Appl. Energy 321 (2022) 119348, https://doi.org/10.1016/j.apenergy.2022.119348.

[37] M. Wang, R. Jing, H. Zhang, C. Meng, N. Li, Y. Zhao, An innovative organic Rankine cycle (ORC) based ocean thermal energy conversion (OTEC) system with performance simulation and multi-objective optimization, Appl. Therm. Eng. 145 (2018) 743–754, https://doi.org/10.1016/j.applthermaleng.2018.09.075.

[38] S. Yi, Z. Zhang, W. Peng, J. Zhang, H. Yuan, Pre-expansion ejector absorption power cycle for ocean thermal energy conversion, Energ. Conver. Manage. 269 (2022) 116151, https://doi.org/10.1016/j.enconman.2022.116151.

[39] C. Fan, Y. Chen, Design optimization of ocean thermal energy conversion (OTEC) considering the off-design condition, J. Therm. Sci. 32 (2023) 2126–2143, https://doi.org/10.1007/s11630-023-1884-x.

[40] G. Wang, Y. Yang, S. Wang, H. Zhang, Y. Wang, Efficiency analysis and experimental validation of the ocean thermal energy conversion with phase change material for underwater vehicle, Appl. Energy 248 (2019) 475–488, https://doi.org/10.1016/j.apenergy.2019.04.146.

[41] Ali Dezhdar, Ehsanolah Assareh, Sajjad Keykhah, Ali Bedakhanian, Moonyong Lee, A transient model for clean electricity generation using solar energy and ocean thermal energy conversion (OTEC) - case study: Karkheh dam - southwest Iran, Energy Nexus 9 (2023) 100176, https://doi.org/10.1016/j.nexus.2023.100176.

[42] S. Lim, J. Yoon, H. Lee, H. Kim, Performance evaluation of control compatibility for an OTEC pump shutdown condition, J. Mar. Sci. Eng. (2023) 11.

[43] C. Xiao, R. Gulfam, Opinion on ocean thermal energy conversion (OTEC), Front. Energy Res. (2023) 11.

[44] E.A. Rad, E. Tayyeban, E. Assareh, et al., Thermodynamic feasibility and multiobjective optimization of a closed Brayton cycle-based clean cogeneration system, J. Therm. Anal. Calorim. (2023), https://doi.org/10.1007/s10973-023-12630-2.

[45] P. Ahmadi, I. Dincer, M.A. Rosen, Multi-objective optimization of an ocean thermal energy conversion system for hydrogen production, Int. J. Hydrogen Energy 40 (2015) 7601–7608, https://doi.org/10.1016/j.ijhydene.2014.10.056.

[46] Mohammad H. Ahmadi, Mehdi Mehrpooya, Fathollah Pourfayaz, Thermodynamic and exergy analysis and optimization of a transcritical CO2 power cycle driven by geothermal energy with liquefied natural gas as its heat sink, Appl. Therm. Eng. 109 (2016) 640–652, https://doi.org/10.1016/j.applthermaleng.2016.08.141.

[47] H. Shoeibi, M. Mehrpooya, E. Assaerh, et al., Graphic analysis of energy and exergy combined systems of solar collector and high-temperature heat pump, Chem. Pap. 77 (2023) 1149–1164, https://doi.org/10.1007/s11696-022-02536-y.

[48] Mohammad Sadegh Esmaeili, Mehdi Mehrpooya, Modeling and exergy analysis of an integrated cryogenic refrigeration system and superconducting magnetic energy

storage, Journal of Energy Storage 73 (2023) 109033, https://doi.org/10.1016/j.est.2023.109033.

[49] Siamak Hoseinzadeh, Heyns, Development of a model efficiency improvement for the designing of feedwater heaters network in thermal power plants, J. Energy Resour. Technol. 144 (7) (2022) 072102, https://doi.org/10.1115/1.4054196.

[50] Siamak Hoseinzadeh, Heyns, Advanced energy, exergy and environmental (3E) analyses and optimization of a coal-fired 400 MW thermal power plant, J. Energy Resour. Technol. 143 (8) (2021) 082106, https://doi.org/10.1115/1.4048982.